sustainability

MDPI

Article

Experimental and Theoretical Study of Methylene Blue Adsorption on a New Raw Material, *Cynara scolymus*—A Statistical Physics Assessment

Chaker Djama [1], Abdallah Bouguettoucha [1,*], Derradji Chebli [1], Abdeltif Amrane [2,*], Hichem Tahraoui [1,3], Jie Zhang [4] and Lotfi Mouni [5]

1 Laboratoire de Génie des Procédés Chimiques, Department of Process Engineering, University of Ferhat Abbas, Setif 19000, Algeria; chaker.djama@univ-setif.dz (C.D.); derradji.chebli@univ-setif.dz (D.C.); hichemm.tahraouii@gmail.com (H.T.)
2 Univ Rennes, Ecole Nationale Supérieure de Chimie de Rennes, CNRS, ISCR—UMR 6226, F-35000 Rennes, France
3 Laboratory of Biomaterials and Transport Phenomena (LBMTP), University Yahia Fares, Médéa 26000, Algeria
4 School of Engineering, Merz Court, Newcastle University, Newcastle upon Tyne NE1 7RU, UK; jie.zhang@newcastle.ac.uk
5 Laboratory of Management and Valorization of Natural Resources and Quality Assurance, SNVST Faculty, University of Bouira, Bouira 10000, Algeria; lotfimouni@gmail.com
* Correspondence: abdallah.bouguettoucha@univ-setif.dz (A.B.); abdeltif.amrane@univ-rennes1.fr (A.A.)

Abstract: Methylene blue (MB) adsorption was performed on a natural material powder of *Cynara scolymus* as a new inexpensive adsorbent identified by Cs. To analyze the Cs material, FTIR, SEM, isoelectric point (pH_{pzc}) analysis, TGA, and DRX were used. The maximum experimental adsorption capacity of the Cs material was 203.333, 192.187, and 179.380 mg•g^{-1} at 298, 303, and 313 K, respectively. The correlation coefficients (R^2) and average percentage errors APE (%) values for the kinetic and isotherms models indicated that the adsorption kinetics followed a pseudo-nth order model and that the traditional isotherm model Redlich–Peterson (R–P) correctly described the experimental data obtained at 298, 303, and 313 K, respectively. The steric, energetic, and thermodynamic characteristics of the most relevant advanced model (double-energy single-layer model (AM 2)) were analyzed in detail. The number of active sites for the first receptors (n_1) was determined to be 0.129, 0.610, and 6.833, whereas the number of second active sites (n_2) was determined to be 1.444, 1.675, and 2.036 at 298, 303, and 313 K, respectively. This indicated the presence of both multi–docking and multimolecular modes for the first style of MB ions (n_1), while only a multimolecular mode for the second style of MB ions (n_2). Thermodynamic characteristics demonstrated that MB adsorption onto the Cs adsorbent is spontaneous and feasible.

Keywords: adsorption; methylene blue; *Cynara scolymus*; isotherm; kinetics; physical models

check for updates

Citation: Djama, C.; Bouguettoucha, A.; Chebli, D.; Amrane, A.; Tahraoui, H.; Zhang, J.; Mouni, L. Experimental and Theoretical Study of Methylene Blue Adsorption on a New Raw Material, *Cynara scolymus*—A Statistical Physics Assessment. *Sustainability* **2023**, *15*, 10364. https://doi.org/10.3390/su151310364

Academic Editor: Chenggang Gu

Received: 18 April 2023
Revised: 13 June 2023
Accepted: 26 June 2023
Published: 30 June 2023

Copyright: © 2023 by the authors. Licensee MDPI, Basel, Switzerland. This article is an open access article distributed under the terms and conditions of the Creative Commons Attribution (CC BY) license (https://creativecommons.org/licenses/by/4.0/).

1. Introduction

Throughout the world, many industries, such as the cosmetic, food, and paper industries, use dyes in large quantities. Most of these dyes are used in the textile industry [1] for their chemical stability and ease of synthesis. The global coloring production is more than 7×10^5 tons per year, with Azo coloration accounting for 60 to 70% of the total [2]. However, there are serious environmental problems with the use of these synthetic dyes. These industrial aqueous effluents may include tinctorial effluents, which may contain chemicals that are toxic to microbial populations as well as toxic or carcinogenic to humans or animals [3].

Methylene blue is not known to be very dangerous, but it can have a variety of side effects. It can cause short periods of fast or difficult breathing if inhaled. Swallowing

by mouth causes a burning sensation and may cause gastritis, diarrhea, nausea, and vomiting [4].

Several physical, chemical, and biological methods have been introduced to remove this type of dye, such as flocculation, electro flocculation, membrane filtration, liquid–liquid extraction, irradiation, coagulation, ion exchange, advanced oxidation, ozonation, and electrochemical destruction [5]. However, due to the high cost of these processes and their limited capacity to adapt to a wide range of dye wastewater, their use is somewhat limited [6].

Consequently, due to its advantages and ease of use, adsorption remains the most used method in recent years [7]. Several materials, including activated carbon and synthetic clay, are used as adsorbents support in this method. The problem with these materials is the high cost of preparation. For this reason, several researchers are trying to find new materials to lower the preparation cost.

Because of their abundance in nature and the simplicity of their transformation into effective adsorbents, biosorbents attract a lot of attention [8]. For instance, lignocellulosic materials (biosorbents) have been proposed for the treatment of colored effluents, such as orange peel [7], cone of Pinusbrutia [1], Stipatenacissima [2] and its fibers [9], cupuassu shell [10], Saw dust and neem bark [11], raw pomegranate [12], Phragmitesaustralis [13], green macro alga [14], and Acorus calamus [15].

Artichoke, or *Cynara scolymus*, is a vegetable of the Asteraceae family largely consumed in the Mediterranean regions. The edible section of the plant is the flower, known as the head, which is protected by leaf sheaths called bracts [16]. The *Cynara scolymus* canning industry produces solid waste, primarily the stems and external bracts of the flowers, which make up 60–80% of the total *Cynara scolymus* flowers and are unfit for human consumption, and it is generally disposed of as cattle feed or green manure [17]. Recently, this artichoke residue biomass has been investigated for potential use as a bioactive adsorbent precursor in a few research works [18,19].

The adsorption of methylene blue onto such adsorbents was estimated using classical models (i.e., Langmuir, Freundlich, Redlich–Peterson (RP), Sips, and Dubinin–Radushkevich isotherms) at equilibrium, and the parameters of these models can provide information on the classification of active sites and elimination capability without inspecting the absorption mechanism of methylene blue [20,21].

In this study, we employed novel physical models developed based on the grand canonical ensemble to relate the macroscopic features of molecules with the adsorption properties of materials [22,23]. These statistical thermodynamics-based models allow for the estimation of parameters such as the removed amount at saturation (Q_e), the number of adsorbed ions per active site (n), the density of receptor sites (N_m), and the uptake energy (E). All of the parameters were evaluated as a function of the temperature, resulting in a more detailed description of the adsorbate–adsorbent adsorption system [24].

The physical parameters collected from the simulation using these models allow us to describe the adsorption process at a molecular level if the adsorbate characteristics, adsorbent porosity, and surface charge are well characterized. Langmuir's model, for example, indicates that the adsorption site accepts one molecule of adsorbate, while physical models indicate that the acceptor site can accept n molecules of the adsorbate [25,26]. In recent years, numerous researchers have employed these physical models to describe the adsorption mechanism of their adsorbent materials, such as; porous heterostructured MXene/biomass activated carbon composites [27], lignin-based activated carbon [28], carbon foam hybrid aerogels [29], organo-sepiolite [30], Alginate/Carbon-based Films [31], cocoa shell [32], bone char [33], Acorus calamus [15], and Binary Mixture of Forest Waste Biopolymer [34]. To our current knowledge, the understanding of the interaction mechanism between *Cynara scolymus* (Cs) direct powder and MB ions remains limited, particularly with regard to utilizing advanced physical models for studying this interaction. Hence, the primary objective of this study is to significantly enhance our understanding by achieving the following key objectives: (a) Assess the adsorption capacity of *Cynara scolymus* direct

powder (Cs) for the effective uptake of MB from aqueous solutions. This investigation will provide valuable insights into the potential of Cs powder as a viable adsorbent for removing MB contaminants. (b) Explore the adsorption properties of MB uptake at various temperatures (298 K, 303 K, and 313 K) using a range of equilibrium equations. By examining the temperature dependence of MB adsorption, we can gain a deeper understanding of the thermodynamics and kinetics of the adsorption process. (c) Analyze the adsorption process by considering classical models, such as Langmuir, Freundlich, Redlich–Peterson (RP), Sips, and Dubinin–Radushkevich isotherms. By applying these well-established models, we can evaluate the adsorption behavior of MB onto the Cs material and compare it with existing literature. (d) Obtain a comprehensive understanding of the underlying mechanism of MB adsorption onto the Cs material by employing statistical physics. This approach will allow us to delve into the microscopic details of the adsorption process and gain insights into the molecular interactions between Cs and MB ions. (e) Define the adsorption phenomena in macroscopic terms by utilizing thermodynamic functions. This analysis will enable us to characterize the energetics and spontaneity of the adsorption process and provide valuable information on the feasibility and stability of MB adsorption onto Cs. It is worth noting that the preparation of Cs direct powder will be a straightforward and cost-effective procedure, ensuring the practicality and applicability of this material for potential environmental remediation applications.

2. Materials and Methods

This research contributes to sustainability in several ways. Firstly, it aims to evaluate the adsorption capacity of Cs direct powder to effectively remove MB from aqueous solutions. By understanding the adsorption properties of Cs, this study can provide valuable insights into its potential as a viable adsorbent for removing contaminants like MB. Developing efficient adsorption materials can contribute to water decontamination and the preservation of water resource quality. Additionally, this research explores the adsorption properties of MB at different temperatures using a range of equilibrium equations. This analysis will improve our understanding of the thermodynamics and kinetics of the MB adsorption process, enabling the optimization of operating conditions for more efficient and energy-saving adsorption processes, thus contributing to the sustainability of water decontamination processes. In this study, classical models such as Langmuir, Freundlich, Redlich–Peterson (RP), Sips, and Dubinin–Radushkevich have been employed to analyze the adsorption process of MB onto Cs. These established models allow for the evaluation of the adsorption behavior and its comparison with existing literature. This evaluation of adsorption models will provide a better understanding of the interactions between Cs and MB ions, facilitating the design of more efficient and sustainable adsorption materials. Furthermore, this research adopts a statistical physics approach to gain a comprehensive understanding of the underlying mechanism of MB adsorption onto Cs. By studying the microscopic details of the adsorption process, researchers can gather insights into the molecular interactions between Cs and MB ions. This in-depth knowledge can be utilized to improve the design of more selective and specific adsorption materials, promoting more efficient and sustainable resource utilization. Finally, this research utilizes thermodynamic functions to characterize the adsorption phenomena on a macroscopic scale. The analysis of thermodynamic properties allows for the determination of the energetics and spontaneity of the MB adsorption process, providing valuable information on the feasibility and stability of MB adsorption onto Cs. This information is crucial for evaluating the practical applicability of Cs as an adsorbent in environmental remediation applications, thereby contributing to the sustainable utilization of resources and environmental preservation.

This research provides in-depth knowledge of the adsorption mechanisms of MB onto Cs direct powder. By improving our understanding of adsorption processes and optimizing adsorption materials, this study contributes to sustainability by advancing water decontamination practices, promoting efficient resource utilization, and preserving the environment.

2.1. Materials

The *Cynara scolymus* biomass (external bracts) waste used in this research was collected after consumption. Hydrochloric acid (HCl) with 35% (*w*/*w*), Sodium hydroxide (NaOH) with 98.8 % (*w*/*w*), sodium chloride (NaCl) with 95% (*w*/*w*), and humic acid (HA) with 99.9% (*w*/*w*) were obtained from Sigma-Aldrich.

2.2. Adsorbent Preparation

Cynara scolymus residue wastes were passed through several stages of crushing, washing drying, grinding, and sieving to produce the final product powder (Cs) used in this work.

Large quantities of collected *Cynara scolymus* were ground, washed multiple times with tap water and then distilled water to remove unwanted impurities, dried in an oven at around 333 K, and finally ground to a uniform powder. The particle sizes utilized in the adsorption tests were selectively separated with sieves with mesh widths ranging from 0.3 to 0.5 mm. The finished powder was kept in a desiccator until needed.

2.3. Effluent Preparation (MB)

Bis-(dimethylamino)–3.7 phenazathionium chloride, or methylene blue as it is commonly named, and containing an ammonium base, was in the form of a dark green powder. Its crude chemical formula is $C_{16}H_{18}ClN_3S$ with a molar mass of 319.85 g•mol^{-1} and solubility of 4 g•L^{-1} at 293 K. All the MB solutions used in this work were prepared from the stock solution at a concentration of 1 g•L^{-1}. All the glassware was washed with distilled water and dried in an oven at 323 K before being used. HCl and NaOH were used to adjust the pH to the desired value. The absorbance of each residual concentration was determined using a UV-vis spectrophotometer SP-8001 from Axiom (Frankfurt, Germany).

2.4. Characterization of the Adsorbent

Various characterization techniques were used in this study and are detailed below.

FTIR analysis allows the determination of functional material surface groups. Infrared spectroscopy was performed on natural and loaded Cs with MB dye (Cs-MB) using the Fourier Transform Infrared spectrometer (FTIR) model IRAffinity-1S from Shimadzu (Nakagyo-Ku, Japan), employing a high-pressure KBr disc technique in the band of 4000 to 400 cm^{-1}.

Additionally, the Cs material fine powder was analyzed using a PW3071/xx diffractometer operating at 45 KV and 35 mA with a copper anticathode emitting Ka radiation (λ = 1.5405 A). The XRD graphs were made with a step of 0.02° and a time step of 6.985 s/step throughout a 2θ angle range of 4 to 90°.

Scanning electron microscopy (SEM) of the Cs product before biosorption was visualized using the JCM-5000 NeoScope TM from Jeol (Tokyo, Japan) to examine the morphological features of the Cs biosorbent.

To evaluate the thermal characteristics of the Cs material, a thermogravimetric examination was performed in the temperature range of 303 to 1053 K using an SDT Q600 V20.9 Build 20 thermal gravimetric from TA Instruments (New Castle, DE, USA).

Finally, electrostatic interactions with a material surface are among the most important factors in deciding on the functionality and compatibility between the adsorbent and the adsorbate to give an idea of the adsorption mechanism. To determine the ph_{pzc} of our materials, a very simple protocol was considered. A series of suspensions: biosorbent (10 mg)/distilled water (10 mL) stirred for 24 h, each with a different initial pH (range 2 to 12), and the final pH was measured. The results are graphically represented (when ΔpH = 0, the pH_{pzc} point equals the pHi).

2.5. Effect of the Initial pH

A factor that plays a very important role in the adsorption phenomenon is pH, which can alter the surface function and the distribution of anions and cations of any material.

To test the effect of this parameter, in each 25 mL Erlenmeyer flask, 10 mL of a methylene blue solution at 250 mg•L^{-1} was mixed with 10 mg of Cs. Every suspension was adjusted to a given initial pH (range of 2.4 to 12).

At room temperature, the mixture was stirred for 24 h at a speed of 250 ppm. The suspension was centrifuged, and the final concentration of the filter was measured by UV.

2.6. Effect of Humic Acid and NaCl

Textile wastewater is known to contain inorganic and organic ions in varying concentrations, mainly cations and anions such as chlorides, nitrates, hydrogen, sulfates, and carbonates. Consequently, and to get information on the effect of these ions on the retention process of MB dye by the Cs material, NaCl and humic acid (HA) have been considered as test ions.

A small amount of NaCl (0.1 M) was added to 10 mL of MB and 10 mg of biosorbent for different concentrations of MB dye (from 50 to 800 mg•L^{-1}). The mixture was stirred until the equilibrium time, and then the suspension was separated and analyzed. The same protocol was repeated with the second HA ion (0.1 M).

2.7. Study of Adsorption

2.7.1. Adsorption Kinetics

The following experiment was performed on three different MB concentrations (50, 100, and 200 mg•L^{-1}). In a 50 mL Erlenemayer series, at optimal pH (pH chosen in the section: pH Influence) and ambient temperature, 20 mg of adsorbent was introduced into 20 mL of MB dye solution. The mixture was stirred for a given time at a speed of 250 rpm on stir plates. Then, the centrifugation of each suspension was centrifuged, and the absorbance was measured to determine the residual MB. The adsorbed quantity was calculated using the following Equation:

$$Q_t = \frac{(C_0 - C_t)V}{m} \quad (1)$$

where Q_t is the quantity adsorbed, C_0 is the initial concentration of MB, C_t is the final concentration of MB, V is the volume of the mixture, and m is the mass of the mixture.

2.7.2. Kinetic Modeling

Some kinetic models such as pseudo-first-order, pseudo-second-order [35], and Pseudo-n^{th}-order [36] were used. Their Equation and parameter are listed in Table 1.

Table 1. Equations of PFO, PSO, and PNO models for nonlinear regression of Kinetic adsorption data.

Kinetics Model	Number	Equation
Pseudo-first order	(2)	$Q_t = Q_e\left(1 - e^{-kt}\right)$
Pseudo-second order	(3)	$Q_t = \frac{k_2 {Q_e}^2 t}{1 + k_2 Q_e t}$
Pseudo-n^{th}order	(4)	$Q_t = Q_e - \left[(no-1)k_{no}t + {Q_e}^{(no-1)}\right]^{\frac{1}{1-no}}$
Intraparticle diffusion	(5)	$Q_t = k_{id}.t^{1/2} + C$
Boyd	(6)	$F_t = \frac{Q_t}{Q_e} = 1 - \frac{6}{\pi^2}e^{-\beta_t}$
	(7)	$\beta_t = -0.4977 - \ln(1 - F)$

The intraparticle diffusion model and the Boyd model were considered to evaluate the diffusion mechanism and the rate control step.

2.7.3. Isotherm Adsorption

The capacity of adsorbents to adsorb the different components of a mixture is the most critical factor in the efficiency of most adsorption processes. Therefore, it is important to have a clear understanding of the properties of the adsorbent-adsorbate equilibrium. For planning and scaling precisely the adsorption process, three isotherms were performed at the three temperatures (T = 298, 303.313 K) by the protocol outlined below.

For each Erlenemayer (25 mL), 10 g of adsorbent was added to 10 mL of MB of variable concentration solution at the optimal pH. The mixture was stirred at 250 ppm up to equilibrium. A wide range of MB concentrations was used (from 50 to 800 mg•L^{-1}).

The adsorbed quantity was determined using Equation (8).

$$Q_e = \frac{(C_0 - C_e)V}{m} \tag{8}$$

where Q_e is the quantity adsorbed, C_0 is the initial concentration of MB, C_e is the final concentration of MB in the solution, V is the volume of the mixture, and m is the mass of the mixture.

2.7.4. Isothermmodeling

Mathematical simulations were carried out to evaluate accurately the interaction between the Cs and the MB dye.

Classical Models

Three models, each with a two-parameter equation, Langmuir, Freundlich, and Dubinin–Radushkevich [37], and two models, each with a three-parameter equation, Redlich–Peterson [38] and Sips [39], are the most widely used models in the literature to describe the nonlinear equilibrium at a constant temperature between the adsorbed pollutant (Q_e) and the rest of the pollutant in solution (C_e). Table 2 shows the equations and parameters of such models.

Table 2. Langmuir, Freundlich, Dubinin–Radushkevich, Redlich–Peterson (R–P), and Sips equations and Equation.

Isotherme Model	Number	Equation
Langmuir	(9)	$\frac{Q_e}{Q_m} = \frac{K_L C_e}{1 + K_L C_e}$
Freundlich	(10)	$Q_e = K_F C_e^{1/nf}$
Sips	(11)	$\frac{Q_e}{Q_m} = \frac{(K_S C_e)^{ms}}{1 + (K_S C_e)^{ms}}$
Redlich–Peterson	(12)	$Q_e = \frac{k_R C_e}{1 + \alpha_R C_e{}^{\beta_R}}$
Dubinin–Radushkevich	(13)	$Q_e = Q_m e^{(-k_{DR}\varepsilon^2)}$ with : $\varepsilon = RT\ln\left(1 + \left(\frac{1}{C_e}\right)\right)$

Advanced Statistical Physics Models for Analyzing the Experimental Results of Adsorption Isotherm of MB on Cs

To better understand the mechanism of MB adsorption on Cs, advanced adsorption models were considered to confirm the results obtained using classical models, as well as to provide more information on the behavior of the adsorbent-adsorbate system [40].

Five advanced models were selected for this analysis. These models are briefly represented in Table 3.

Table 3. The Advanced statistical physics models AM1, AM2, AM3, AM4, and AM5.

Model	Num	Equation	Ref
Single-energy single-layer model (AM1)	(14)	$Q_e = \frac{Q_0}{1 + \left(\frac{C_{1/2}}{C_e}\right)^n} = \frac{n.N_m}{1 + \left(\frac{C_{1/2}}{C_e}\right)^n}$	[38]
Double-energy single-layer model (AM 2)	(15)	$Q_e = \frac{n_1.N_{m1}.}{1 + \left(\frac{C_1}{C_e}\right)^{n_1}} + \frac{n_2.N_{m2}}{1 + \left(\frac{C_2}{C_e}\right)^{n_2}}$	[39]
Single-energy double-layer model (AM 3)	(16)	$Q_e = n.N_m.\frac{\left(\frac{C_e}{C_{1/2}}\right)^n + 2.\left(\frac{C_e}{C_{1/2}}\right)^{2n}}{1 + \left(\frac{C_e}{C_{1/2^1}}\right)^n + \left(\frac{C_e}{C_{1/2}}\right)^{2n}}$	[20]

Table 3. *Cont.*

Model	Num	Equation	Ref
Double-energy double-layer model (AM 4)	(17)	$Q_e = n.N_m.\frac{\left(\frac{C_e}{C_1}\right)^n + 2.\left(\frac{C_e}{C_2}\right)^{2n}}{1 + \left(\frac{C_e}{C_1}\right)^n + \left(\frac{C_e}{C_2}\right)^{2n}}$	[21]
Finitemultilayer (AM 5)	(18)	$Q_e = n.N_m.\frac{F_1(C_e) + F_2(C_e) + F_3(C_e) + F_4(C_e)}{G(C_e)}$ With: $F_1(C_e) = \frac{\left(-2.\left(\frac{C_e}{C_1}\right)^{2n}\right)}{\left(1-\left(\frac{C_e}{C_1}\right)^n\right)} + \frac{\left(\frac{C_e}{C_1}\right)^n\left(1-\left(\frac{C_e}{C_1}\right)^{2n}\right)}{\left(1-\left(\frac{C_e}{C_1}\right)^n\right)^2}$ $F_2(C_e) = \frac{2.\left(\frac{C_e}{C_1}\right)^n\left(\frac{C_e}{C_2}\right)^n\left(1-\left(\frac{C_e}{C_2}\right)^{(nN_2)}\right)}{\left(1-\left(\frac{C_e}{C_2}\right)^n\right)}$ $F_3(C_e) = \frac{-\left(\frac{C_e}{C_1}\right)^n\left(\frac{C_e}{C_2}\right)^n\left(\frac{C_e}{C_2}\right)^{(nN_2)}N_2}{\left(1-\left(\frac{C_e}{C_2}\right)^n\right)}$ $F_3(C_e) = \frac{\left(\frac{C_e}{C_1}\right)^n\left(\frac{C_e}{C_2}\right)^{(2n)}\left(1-\left(\frac{C_e}{C_2}\right)^{(nN_2)}\right)}{\left(1-\left(\frac{C_e}{C_2}\right)^n\right)^2}$ $G(C_e) = \frac{\left(1-\left(\frac{C_e}{C_1}\right)^{(2n)}\right)}{\left(1-\left(\frac{C_e}{C_1}\right)^n\right)} + \frac{\left(\frac{C_e}{C_1}\right)^n\left(\frac{C_e}{C_2}\right)^n\left(1-\left(\frac{C_e}{C_2}\right)^{(nN_2)}\right)}{\left(1-\left(\frac{C_e}{C_2}\right)^n\right)}$	[39]

2.8. Statistical Assessment of Equilibrium Parameters

The average percentage errors APE (%) function, represented by Equation (19), was used to evaluate nonlinear adsorption curves of kinetics and isotherms. This function allows comparing experimental data to the adjusted model's results point by point. The models with the lowest APE (%) values are the best for describing the experimental behavior.

$$APE(\%) = \frac{\sum_{i=1}^{N} \frac{|Qi.mod - Qi.exp|}{Qi.exp}}{N} \times 100 \quad (19)$$

where Qi.mod is the model's adsorption capacity, Qi.exp is the experimental adsorption capacity, and N is the number of experimental points performed [40].

3. Results and Discussion

3.1. Adsorbent Characterization

The FTIR analysis was utilized to determine the functional groups existing on the *Cynara scolymus* surface (Cs) material before and after the adsorption of MB color (Cs-MB). The acquired results are depicted in Figure 1a.

Broadband between 3700 and 3000 cm^{-1} demonstrated that the surface of Cs contains a greater amount of alcoholic and phenolic –OH functional groups than cellulose, Pectin, and lignin in powder of leaf structure [41]. The peak at 2939 cm^{-1} correlated to the methyl group's C–H stretching bond [42]. The peak at 1745 cm^{-1} corresponded to the bending of the C=O functional group found in quinones and lactones. The sharp peak at 1648 cm^{-1} was associated with the bending vibrations of C=O derived from a carboxylic acid [43]. The peak at 1429 cm^{-1} was assigned to the carboxylate functional group (COO^-). The peak at 1256 cm^{-1} was associated with the bending modes of the ligands O–C–H, C–C–H, and C–O–H. A prominent band of about 1036 cm^{-1} verified the presence of the functional group C–O–C in the cellulose and lignin molecules of Cs [44]. These functional groups on the Cs surface could serve as active sites for cationic dye adsorption. Figure 1a illustrates the changes in FTIR spectra caused by dye adsorption. There was a considerable drop in the strength of the C–H and C–O–C peaks at 2939 cm^{-1} and 1036 cm^{-1}, respectively, which could be due to MB adsorption onto Cs adsorbent [7].

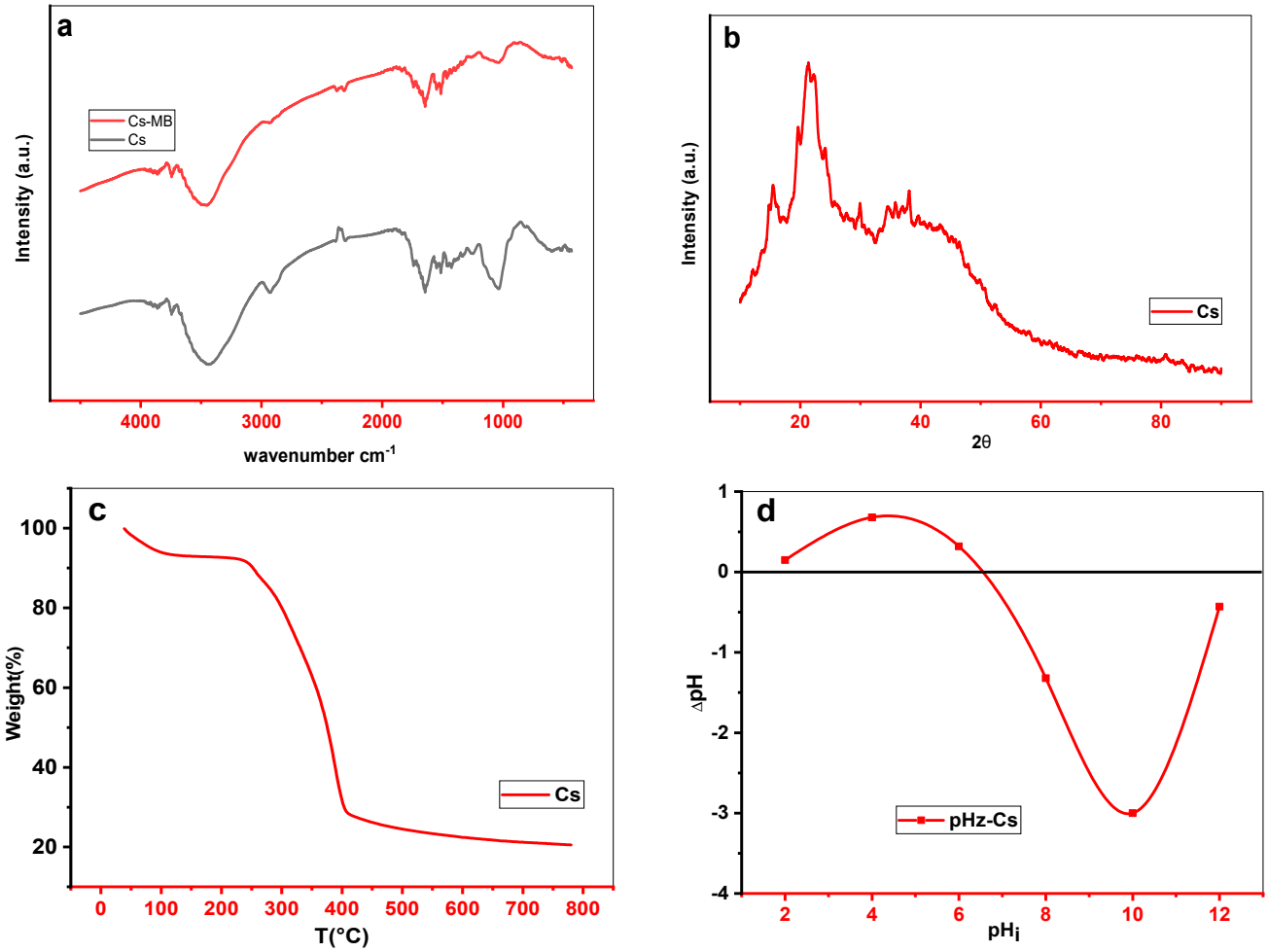

Figure 1. *Cynara scolymus* (Cs) Characterization (**a**) FTIR spectrum, (**b**) XRD shape, (**c**) Thermogravimetric analysis, (**d**) isoelectric point.

Figure 1b depicts the XRD pattern for Cs. As can be seen, the sample diffraction pattern had two planes at approximately 15° and 21°2θ. The plane (0 0 2) of cellulose I was responsible for a high-intensity peak near 21.5° at 2θ. The plane (1 0 1) of cellulose I, which was near 15.5°, exhibited significantly less diffraction and overlap. This could be due to the comparatively large concentrations of lignin and hemicellulose in natural lignocellulose Cs. which contribute to its amorphous nature [44,45].

The thermogravimetric analysis (TGA) results are displayed in Figure 1c. Thermal analysis revealed two regions; the first suggested that the Cs biomass lost weight between 35 and 230 °C as a result of moisture evaporation. The second zone was 230–400 °C and demonstrated the greatest weight loss due to hemicellulose and cellulose degradation. The final weight reduction was at 450 °C, which was entirely due to lignin degradation [46].

From Figure 1d, the pH_{pzc} of the Cs substance was 6.55. Therefore, above this value, the surface of this material was negatively charged by the excess of OH^- anions, and the surface was positively charged below this value by the excess of H^+cations [47].

Figure 2e1–e3 show SEM surface images of the Cs product before adsorption on a scale of 10, 20, and 50 µm, respectively, and Figure 2f1–f3 after adsorption. Figure 2e1–e3 revealed a heterogeneous surface structure with many cavities of varying sizes. As a result of the irregular morphology of the material, we can deduce that the Cs material represented a suitable morphological profile for dye adsorption. After adsorption and from Figure 2f1–f3, the coverage of the adsorbent surface (Cs) due to the adsorption of adsorbate molecules (MB), presumably leading to the formation of a monolayer of adsorbate molecules on the

adsorbent surface, is visible from the formation of a white spreading layer (molecular cloud) of uniform thickness and coverage [48].

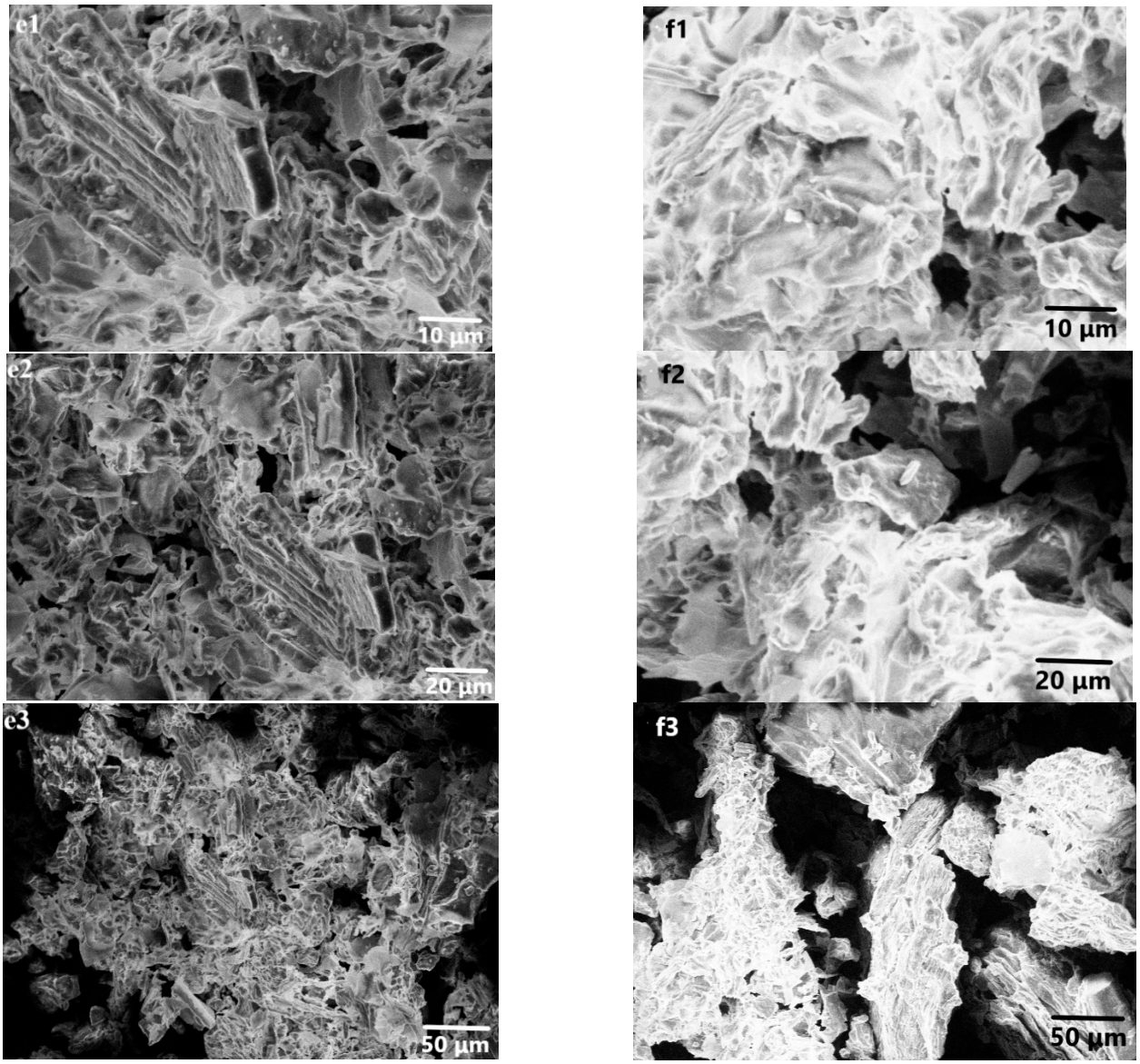

Figure 2. SEM images (**e1**–**e3**) before and (**f1**–**f3**) after adsorption.

3.2. Effect of the Initial pH on Adsorption of MB with Cs

The pH impact of the aqueous solution on MB adsorption on Cs material is shown in Figure 3, which shows a very weak adsorbed quantity for a very low pH range (pH < pH_{pzc}). This may be due to the repulsion force between the positively charged Cs product and the MB cationic dye. The adsorption capacity increased significantly as the pH of the solution increased as a result of an increase in negative charges (OH^- ions) [49] on the Cs surface as the pH increased. At pH 10, the maximum capacity was reached. This confirms that electrostatic interaction plays a significant role in MB adsorption on Cs. We observed a decrease in the adsorbed amount of MB between 10 and 12 pH as a result of the modification of the MB structure in this interval, where the maximum wavelength decreases from 654 to about 550 nm. By these findings, a pH of 10 was considered thereafter.

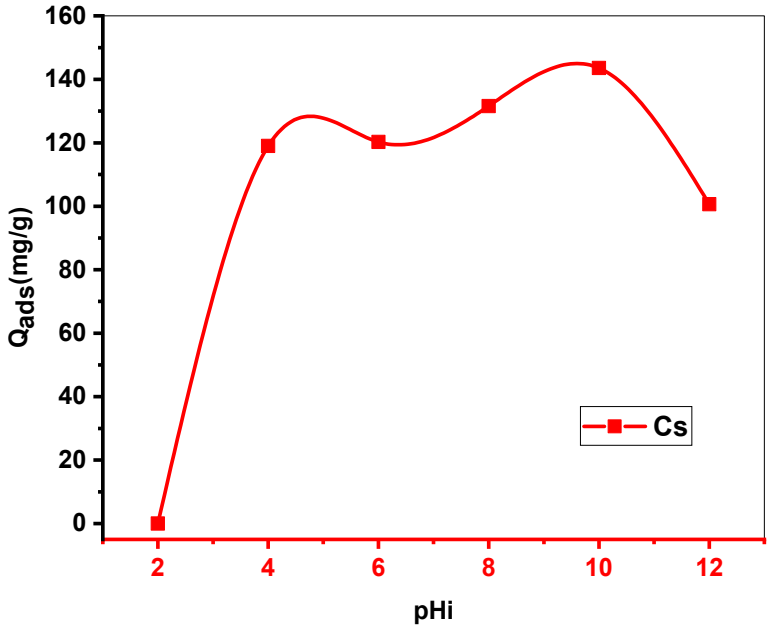

Figure 3. The effect of initial pH on adsorption of MB with Cs (m = 10 mg, V = 10 mL, pH = 10, stirring = 250 ppm, Tambient).

3.3. Influence of Humic Acid (HA) and NaCl on Adsorption of MB on Cs

In the presence of NaCl, the quantity adsorbed (Q_e) decreased from a maximum value of 203 mg•g^{-1} to 180 mg•g^{-1}. As shown in Figure 4, the competitiveness of adhesion onto adsorbent between MB cationic molecules and the Na^+ cations of the inorganic salt was most likely the reason for this decrease.

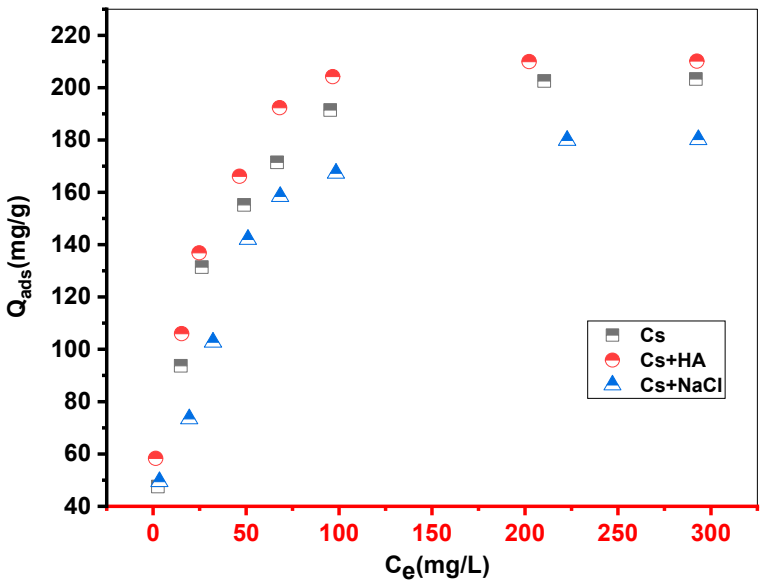

Figure 4. Influence of NaCl and humic acid (HA) on the discoloration of MB solutions by Cs (m = 10 mg, V = 10 mL, stirring = 250 ppm, pH = 10, Tambient).

In the presence of HA, there was a slight rise in the amount of adsorbed MB (Figure 4), and the amount adsorbed (Q_e) increased from 203 mg•g^{-1} to 210 mg•g^{-1}. It can be said that there is no effect of HA in the MB adsorption process. There are two possible explanations for this result: the first is that HA interacts directly with the MB [50], and the second is that HA can create other active sites on the adsorbent Cs where the MB molecules can be captured.

3.4. Kinetics Analysis

From the graph presented in Figure 5, the studied material showed three phases of adsorption kinetics:

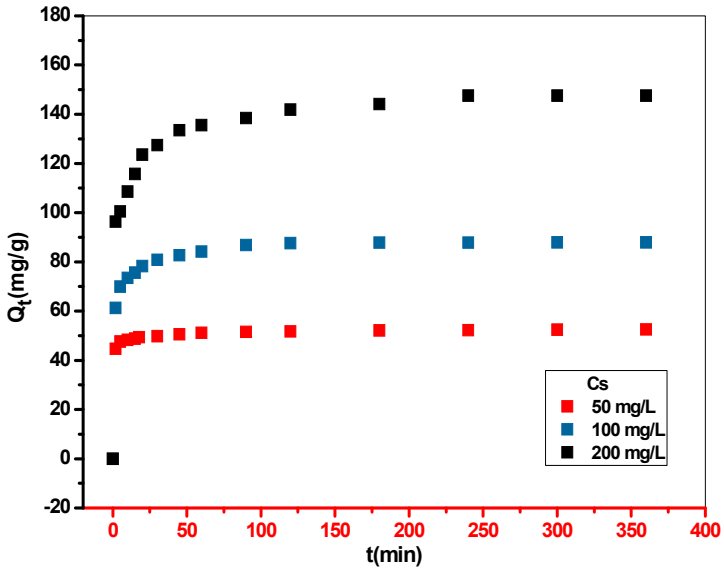

Figure 5. Representative curve of experimental adsorption kinetics of MB on Cs material (m = 10 mg, V = 10 mL, stirring = 250 ppm, pH = 10, Tambient).

The first phase displays a higher removal rate of MB due to vacant adsorbent sites and the large concentration gradient at the beginning of the process. A slower adsorption rate when the solute is adsorbed owing to decreased adsorption sites and gradient concentration in the second phase. The third phase is the saturation or equilibrium step, where there are no more accessible adsorption sites; the beginning of this step is indicated by the equilibrium time, and it was equal to 120 min in our case.

There was also an increase in the quantity adsorbed when the initial concentration of MB increased due to the driving forces, which increased with the initial concentration [51,52].

The Boyds equation was applied to determine the actual control phase. If the plots describe linear simulation for the Boyd model line crossing the origin, then the control phase is the intraparticle diffusion step. If not, the adsorption process is controlled by the film diffusion step [49]. From Figure 6, the $B_t$vs t curves were not linear and did not cross the origin, suggesting that the film diffusion step controlled the adsorption process [53,54].

Figure 7 illustrates the results of the nonlinear regression of the PFO, PSO, and PNO equations, and the corresponding parameters are collected in Table 4. At the initial stages and for the three concentrations (50, 100, and 150 mg•L^{-1}), the PFO-derived curves are above the experimental adsorption data (less than 60 min). On the contrary, they are lower than the experimental data for the final stage of adsorption. The same observation holds for the PSO-derived curves with a slight difference in the initial stage time (less than 100 min). As a result, there exists an order n other than 1 and 2 that provides the lowest deviation throughout the adsorption process [32], as shown by the PNO-derived curves that have the least deviation from the experimental data and confirmed through the values of the correlation coefficients R^2 and the average percentage errors APE (%) given in Table 4. The pseudo-nth-order kinetic model accurately fitted the experimental data and outperformed the pseudo-first and pseudo-second-order equations. The order of adsorption reaction n was found to be between 4.97, 4.365, and 8.04 for 50, 100, and 150 mg•L^{-1} concentrations, respectively. All these results are clearly proved with the two Figures 8 and 9, digital photographic images of a series of adsorption of MB with Cs material and UV-Visible spectrophotometer adsorption of MB for each time interval.

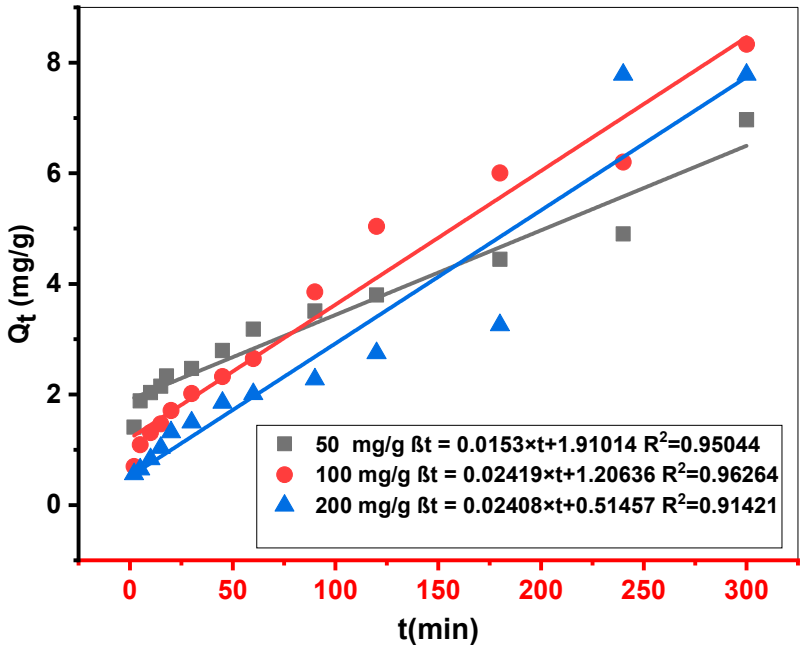

Figure 6. The curves representative of linear simulation of MB adsorption on Cs using the Boyd model.

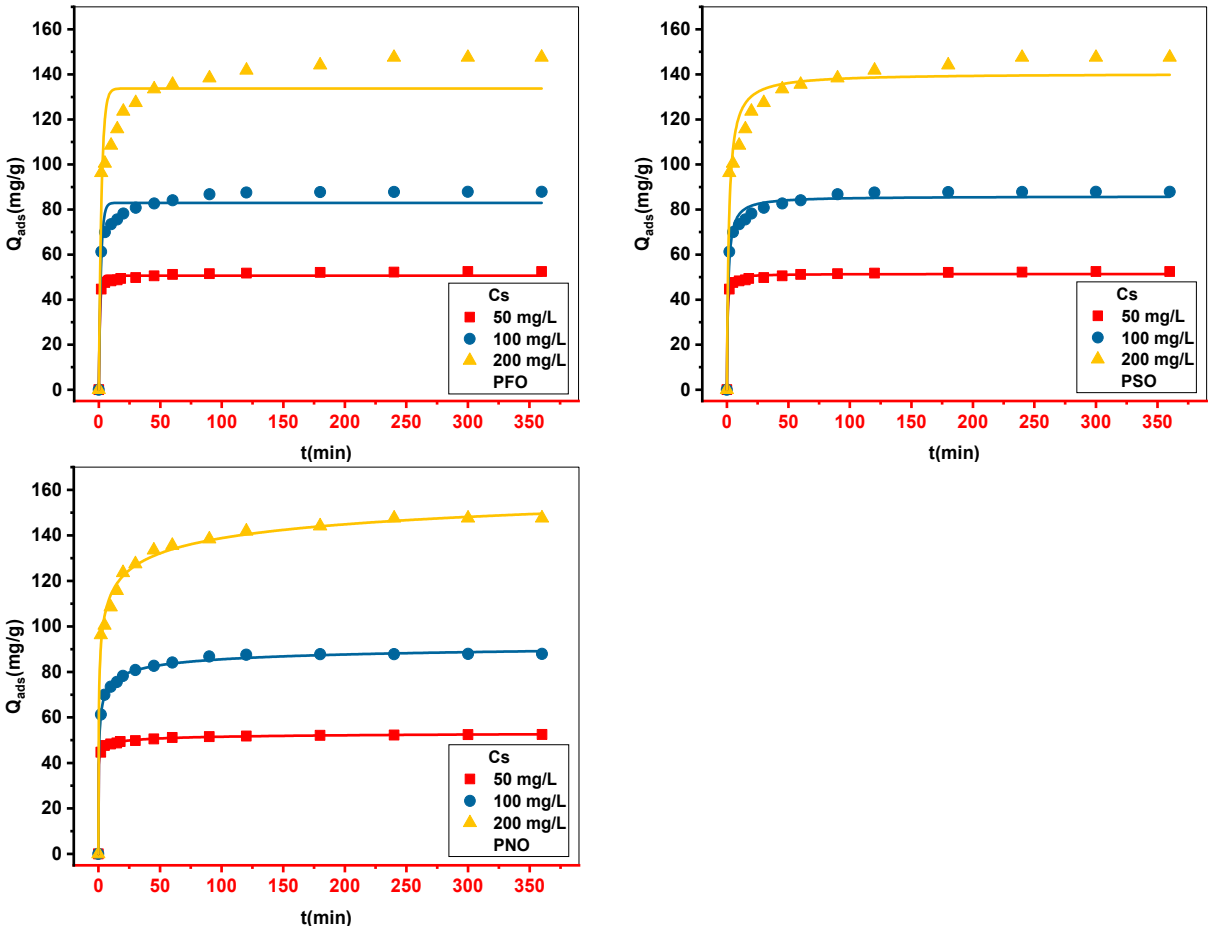

Figure 7. The curves representative of nonlinear simulation of the pseudo-first-order (PFO), pseudo-second-order (PSO), and pseudo-nth-order kinetic models (PNO).

Table 4. Parameters of Kinetic for nonlinear regression of PFO, PSO, and PNO models for the adsorption of MB on Cs.

Models	Parameters	50 mg•L^{-1}	100 mg•L^{-1}	150 mg•L^{-1}
PFO	Qexp	52.5	87.92	147.61
	Q_e	50.68	82.98	133.75
	K_1	1.044	0.58	0.461
	R^2	0.985	0.939	0.865
	APE (%)	2.664	5.973	9.474
PSO	Q_e	51.43	85.88	140.42
	$K_2 \times 10^{+4}$	0.055	0.011	0.0046
	R^2	0.994	0.982	0.947
	APE (%)	1.657	5.714	5.795
PNO	Q_e	55.46	96.89	203.56
	k_n	1.073×10^{-5}	8.38×10^{-7}	2.49×10^{-16}
	no	4.97	4.365	8.04
	R^2	0.999	0.998	0.994
	APE (%)	0.328	0.889	1.851

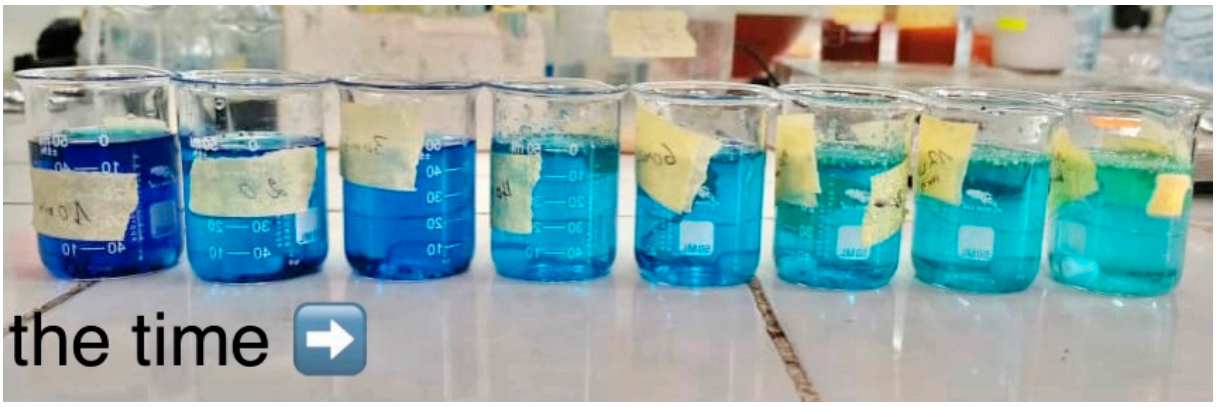

Figure 8. Sequence of digital photographs proving MB adsorption with Cs material.

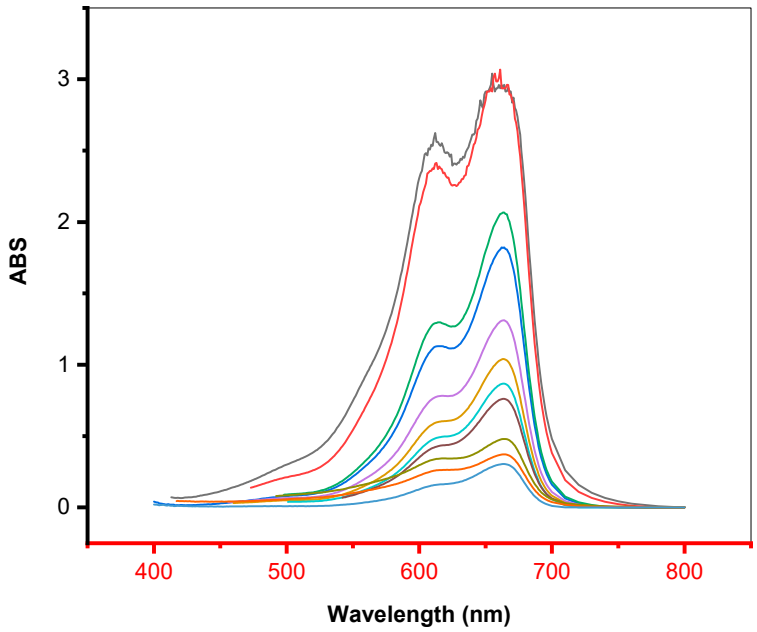

Figure 9. UV-Visible spectrophotometer sorption of MB for each time interval.

3.5. Isotherms Analysis

Figure 10 illustrates the MB dye adsorption isotherm on Cs. The adsorption capacity increased with the initial dye concentration until equilibrium was reached. The adsorption ability of MB on Cs decreased as the temperature increased (the adsorption amounts at temperatures of 298, 303, and 313 K were 203.33, 192.188, and 179.38 mg•g^{-1}, respectively). These results suggest an exothermic MB-Cs adsorption mechanism [51,55,56].

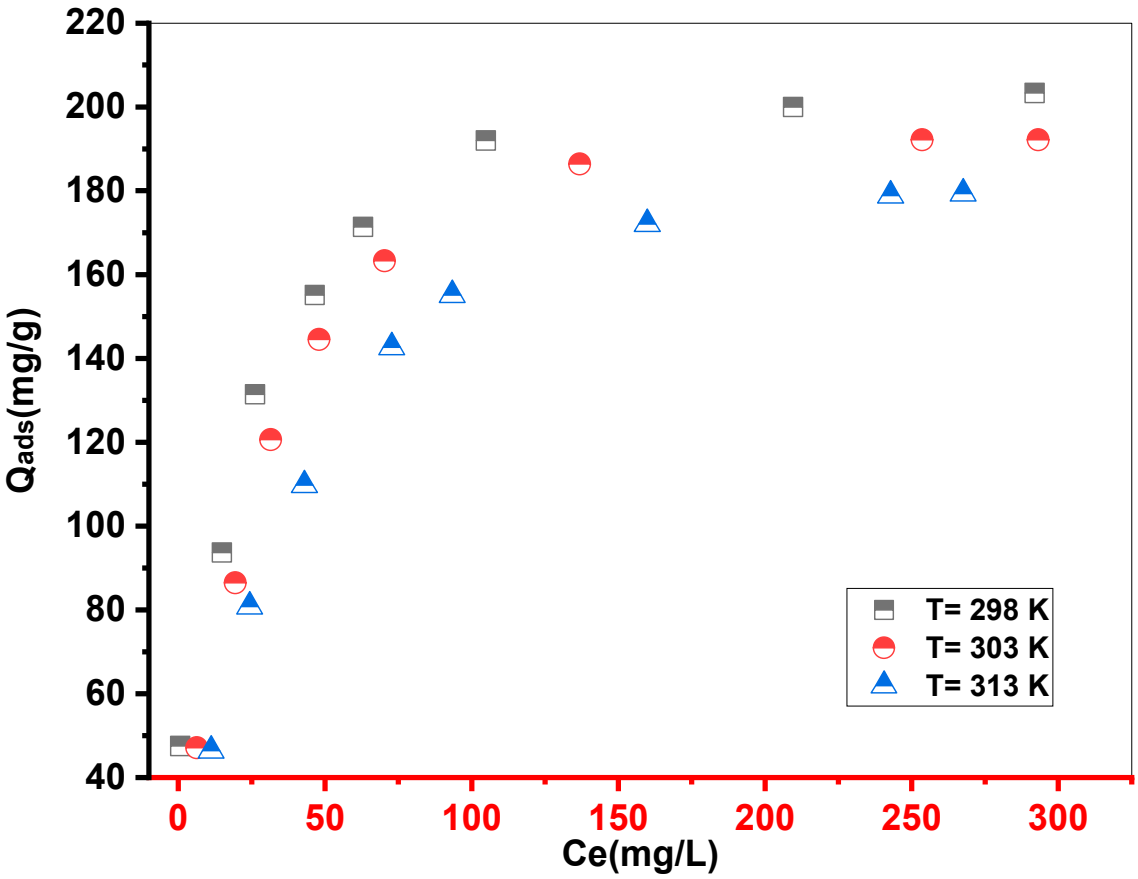

Figure 10. Experimental isotherms of MB adsorption onto Cs. (m = 10 mg, V = 10 mL, stirring = 250 ppm, pH = 10, $T_{ambient}$).

3.5.1. Classical Models

Figure 11 depicts the nonlinear regression findings of the five models Langmuir, Freundlich, Dubinin–Radushkevich (D–R), Redlich–Peterson (R–P), and Sips, and Table 5 provides the fitting parameters as well as the average percentage of errors APE (%) for each. By comparing the R^2 and APE% values, the Redlich–Peterson isotherm model gave the best result of adjusting the MB adsorption on the Cs adsorbent. Because of the three parameters involved in the R–P model, Several studies [51,55] have shown its relevance in describing the adsorption process. It can be noted that the Freundlich and Langmuir isotherms can be derived from the R–P isotherm based on the b_R value. It becomes the Langmuir isotherm when b_R = 1 and the Freundlich isotherm for b_R = 0. The b_R values were very close to unity for the three temperatures tested, indicating that the R–P model was close to the Langmuir model in our adsorption case.

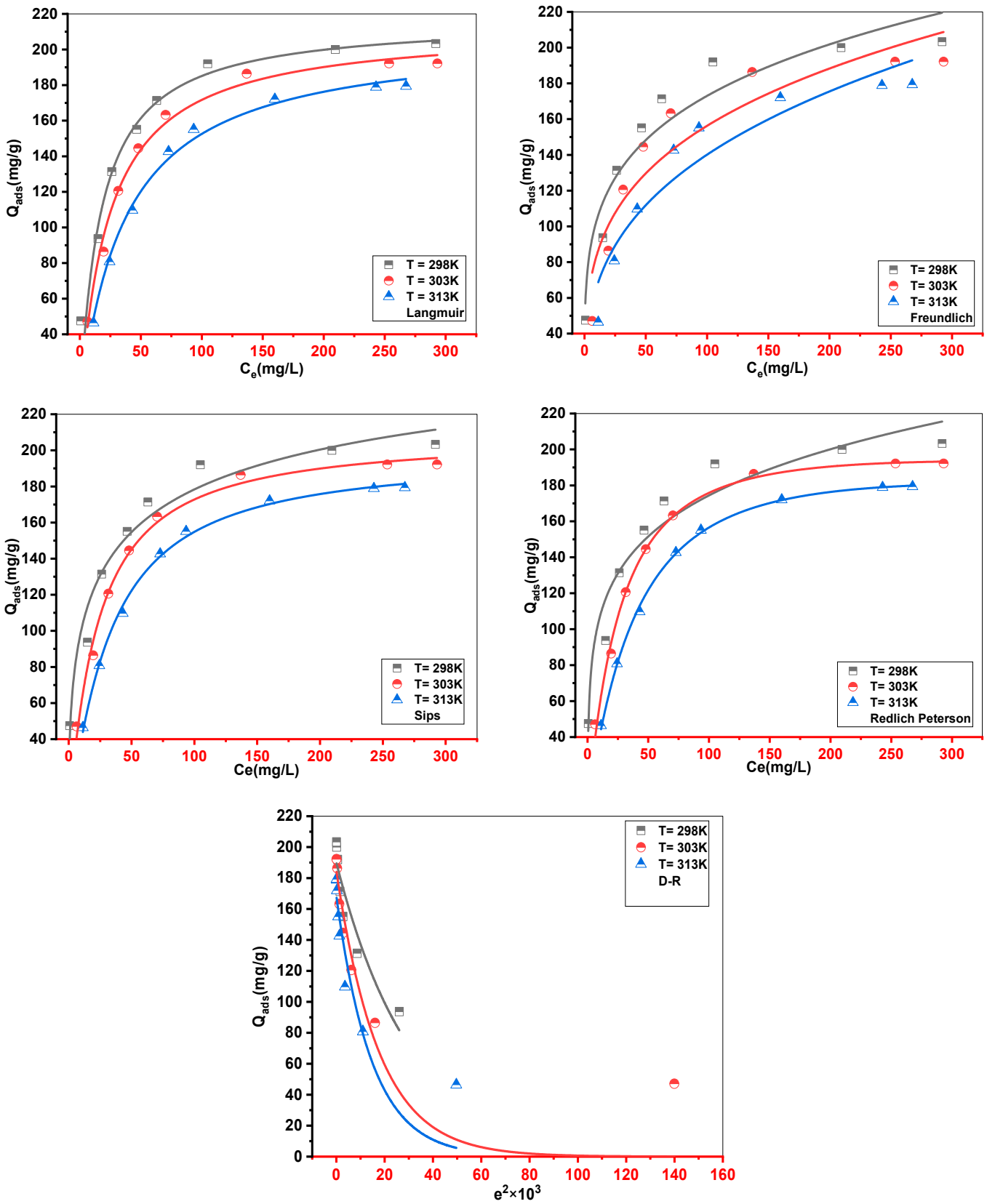

Figure 11. Result of fitting isotherms data of MB adsorption onto Cs with Langmuir, Freundlich, D–R, Redlich–Peterson (R–P), and Sips.

Table 5. Langmuir, Freundlich, D–R, Redlich-Peterson (R–P), and Sips parameters for the adsorption of MB onto Cs.

Models	Parameters	298 K	303 K	313 K
Langmuir	Q_e (mg•g^{-1})	203.333	192.187	179.380
	Q_m (mg•g^{-1})	217.075	213.012	208.577
	K_L (L•mg^{-1})	0.0579	0.04155	0.0272
	R^2	0.911	0.990	0.994
	APE (%)	12.143	3.506	2.707
Freundlich	nf	4.499	3.7136	3.078
	K_F (mg•g^{-1}) (L/mg)$^{1/n}$	62.16	45.219	31.38
	R^2	0.926	0.866	0.899
	APE (%)	9.569	15.586	12.618
Sips	Q_m (mg•g^{-1})	294.691	208.441	197.356
	K_S (L•mg^{-1})	0.0248	0.04314	0.031
	ms	0.4714	1.0793	1.1606
	R^2	0.949	0.989	0.996
	APE (%)	7.645	3.908	1.994
Redlish–Peterson	k_R (L•g^{-1})	181.46	7.294	4.637
	β_R	2.496	0.022	0.011
	R^2	0.926	0.993	0.999
	APE (%)	7.544	3.187	1.224
D–R	Q_m (mg•g^{-1})	189.969	184.75	168.348
	E (kJ•mol^{-1})	3.927	2.967	2.7048
	R^2	0.869	0.832	0.819
	APE (%)	10.614	18.477	17.246

The E values obtained from the Dubinin–Radushkevich (D–R) model were <8.0 kJ•mol^{-1}, confirming the physical nature of the MB adsorption onto the Cs material at all examined temperatures.

The five traditional models considered are insufficient to construct the MB uptake dynamic, and so theoretical treatment via advanced models appears to be a required tool to support the setup/management of the MB–Cs interaction.

3.5.2. Advanced Statistical Physics Models

The simulation of the experimental isotherm data was performed using the software ORIGIN (version 2018) (Figure 12). The choice of the most relevant model(s) for understanding the MB adsorption process onto the Cs material depended on the APE (%) values and correlation coefficient R^2 given in Table 6.

The best advanced statistical physics model for fitting the MB adsorption onto the Cs adsorbent was found to be the AM2 (double-energy single-layer model), which was therefore considered thereafter.

3.5.3. Steric and Energetic Parameters

The physicochemical parameters governing the interaction between MB ions and the Cs material were calculated and intensively interpreted according to the AM2 model in the following sections.

n. N_m. and Q_{ads} Steric Parameter Interpretation

The n value can be used to determine the geometric position (vertical or horizontal) and mechanism (multi–ionic or multimolecular) of the trapped MB ions on the Cs adsorbent surface. When n is less than 1, the adsorbed molecule adopts a parallel (horizontal) orientation with a multi–docking mode. When n is more than 1, the adsorbed molecules are anchored in a non-parallel (vertical) orientation with a multimolecular mode [21,23,39].

Figure 13a depicts n_1 and n_2 as the temperature goes up from 298 to 313 K, and the obtained values of these parameters are shown in Table 6. The n_1 was found to be 0.129, 0.610, and 6.833, while the n_2 values were 1.444, 1.675, and 2.036 at 298, 303, and 313 K, respectively.

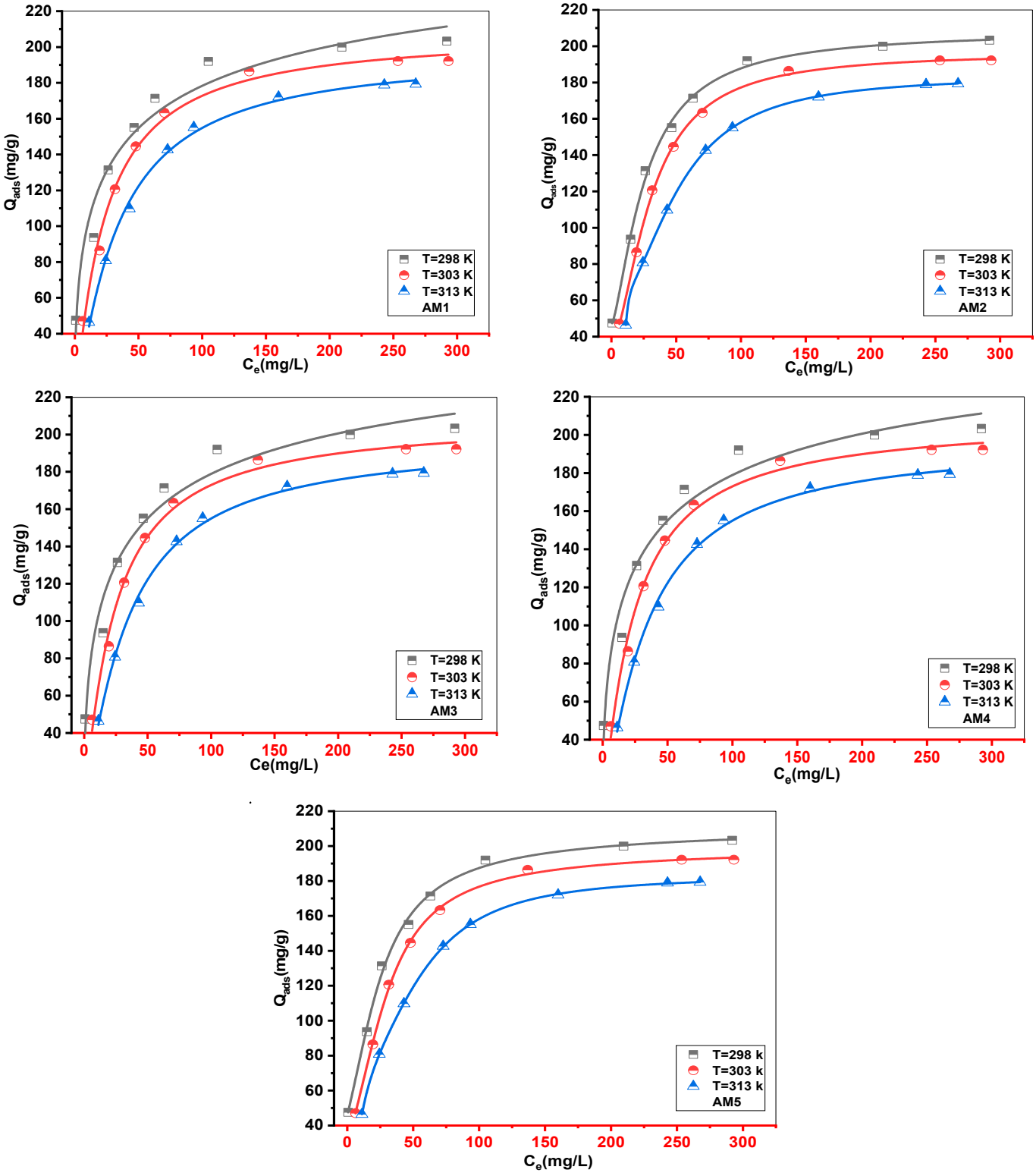

Figure 12. Result of fitting isotherms data of MB adsorption onto Cs with AM1, AM2, AM3, AM4, and AM5 models.

Table 6. Values of the estimated parameters of models AM1, AM2, AM3, AM4, and AM5 of the MB-Cs adsorption process.

Models	Parameters	T = 298 K	T = 303 K	T = 313 K
AM1	n	0.471	1.079	1.161
	N_m	624.728	193.109	170.044
	$C_{1/2}$	40.359	23.182	32.839
	R^2	0.949	0.989	0.996
	APE (%)	7.646	3.908	1.995
AM2	n_1	0.129	0.610	6.833
	n_2	1.444	1.676	2.036
	N_{m1}	360.902	59.874	8.5241
	N_{m2}	112.073	95.507	61.579
	C_1	2.419×10^{-35}	9.807×10^{-13}	9.851
	C_2	26.414	30.566	51.191
	R^2	0.99218	0.99781	0.99994
	APE (%)	1.354960	0.766527	0.096792
AM3	n	0.374	0.811	0.867
	N_m	382.960	130.008	115.298
	$C_{1/2}$	35.781	23.896	33.782
	R^2	0.95233	0.99038	0.99675
	APE (%)	7.527145	3.706916	1.792957
AM4	n	0.363	0.76608	0.81213
	N_m	394.458	137.7444	123.15063
	C_1	45.7492	30.3144	43.7831
	C_2	35.848	23.911	33.791
	R^2	0.94044	0.98802	0.99596
	APE (%)	7.519079	3.701431	1.805403
AM5	n	0.717	0.779	1.986
	N_2	3.842	4.176	1.334
	C_1	1.229×10^{-11}	0.835	9.879
	C_2	27.059	31.696	58.628
	N_m	61,556	49,993	39,537
	R^2	0.99421	0.99812	0.9999
	APE (%)	1.405965	0.8529428	0.17386

At 298 and 303 K, the MB–Cs interaction revealed a horizontal orientation and multi–docking mechanism for the n_1. The adsorbed MB behavior was changed to vertical positioning and multimolecular mode by increasing the solution temperature to 313 K. The second parameter, n_2, displayed a vertical setting and multimolecular mode for the three temperatures. When the temperature increases, the two parameters n_1 and n_2 increase [54,57], as illustrated in Figure 13a. This result demonstrated that the chemical behavior of the MB molecules in solution was the same and that the two parameters, n_1 and n_2, were aggregated but to different degrees (lower degree for the second parameter, n_2). This behavior could be related to the enhanced thermal agitation, which may have resulted in thermal collisions between the MB molecules, increasing the number of captured MB molecules per site.

Figure 13b shows the density (N_m) of the receptor site as a function of temperature. The density of the Cs receptor sites N_{m1} and N_{m2} was reduced as the temperature increased. This evolution is connected to an increase in the number of trapped molecules n_1 and n_2 per site as the temperature increases (the tendency to aggregation) [38,58].

The total saturation adsorption amount (Q_e) is affected by the number of captured molecules per site and the density of receptor sites ($Q_{ei} = N_{mi} \times n_i$), and the total Q_e is the sum of Q_{ei}, this value measures the ability of the Cs surface ability to retain the MB molecules.

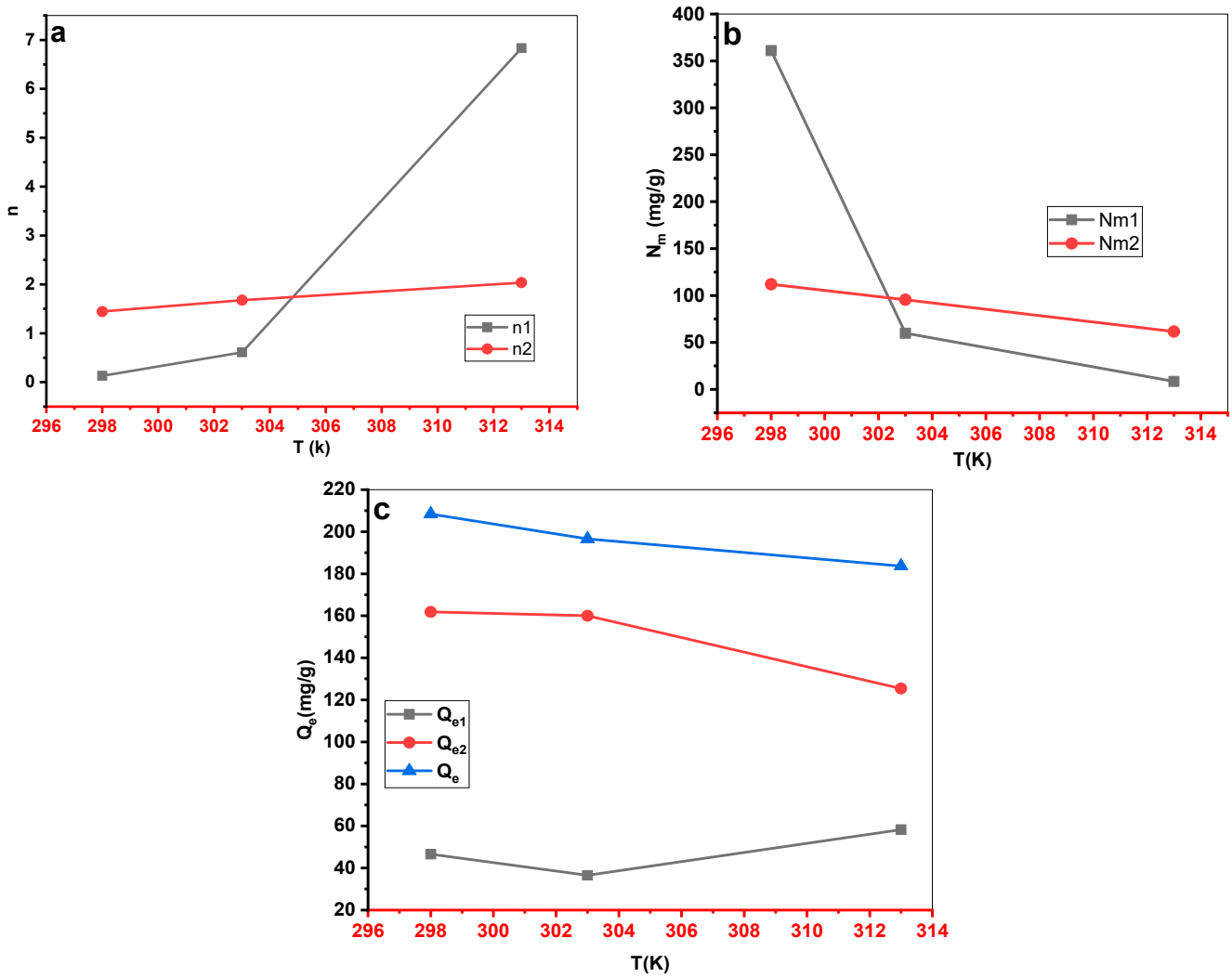

Figure 13. The evolution of (**a**) n, (**b**) N_m, and (**c**) Q_e as a function of temperature for MB-Cs adsorption.

The total amount of saturation adsorption (Q_e) was plotted as a function of temperature in Figure 13c, showing that this parameter was significantly affected by the temperature alteration. Indeed, when the temperature rose, the amount adsorbed decreased due to exothermic adsorption, as is usual in classical adsorption phenomena.

Energetic (E) Parameter Interpretation

The energetic interaction (E) between the MB ions and the Cs surface was calculated using the following equations [59]:

$$C_1 = C_{SM} e^{\frac{-E_1}{RT}} \tag{20}$$

$$C_2 = C_{SM} e^{\frac{-E_2}{RT}} \tag{21}$$

where C_1 and C_2 are the half-saturation concentrations, and C_{SM} is the adsorbate (MB) solubility.

This solubility was considered to remain constant at all adsorption temperatures for simplicity [52]. The solubility was assumed to be constant at all adsorption temperatures.

According to Table 6, the C_1 concentrations at the two temperatures, 298 and 303 K, were found to be relatively low, resulting in inconsistent E_1 values. In this instance, we chose to interpret the energy according to the last temperature (313 K) [52].

For 313 K, the calculated energies were −2.345 kJ•mol^{-1} for the first type of energy (E_1) and −6.633 kJ•mol^{-1}for the second type of energy (E_2). It was discovered that the first energy was lower than the second, demonstrating that the free active sites of the first type were the most prevalent. Moreover, the calculated energy values were low and <40 kJ/mol [47]. As a result, MB adsorption on the Cs adsorbent corresponds to a physical process with the expected existence of a van der Waals interaction or hydrogen bonding.

3.5.4. Thermodynamicynamic Function Study

To conduct a thermodynamic investigation of the MB adsorption mechanism on the Cs materials, the advanced double-energy single-layer model (AM2) could be used to calculate thermodynamic parameters, including entropy, Gibbs free enthalpy, and internal energy [20,21,60].

Entropy

The adsorption process can provide useful information on the order and/or disorder of the adsorbed ions (MB) on the Cs-material through the examination of configurational entropy (i.e., the degree of regularity of the adsorption system). The entropy variation of the second, advanced model as a function of the adsorbate equilibrium concentration is given in Table 7 by Equation (22) [61,62].

Table 7. Entropy, free enthalpy, and internal energy function according to the AM2 model.

Function	Num	Equation
Entropy	(22)	$\frac{S_a}{K_B} = N_1\left[\ln\left(1+\left(\frac{C_e}{C_1}\right)^{n_{1m}}\right)+\frac{n_1\ln\left(\frac{C_1}{C_e}\right)}{1+\left(\frac{C_1}{C_e}\right)^{n_{1m}}}\right]+N_2\left[\ln\left(1+\left(\frac{C_e}{C_2}\right)^{n_2}\right)+\frac{n_2\ln\left(\frac{C_2}{C_e}\right)}{1+\left(\frac{C_2}{C_e}\right)^{n_2}}\right]$
Gibbs free enthalpy	(23)	$G = K_B T\ln\left(\frac{C_e}{Z_v}\right)\left[\frac{Q_{sat1}}{1+\left(\frac{C_1}{C_e}\right)^{n_{1m}}}+\frac{Q_{sat2}}{1+\left(\frac{C_2}{C_e}\right)^{n_{2m}}}\right]$ With: $Z_v = \frac{Z_{gtr}}{V} = \left(\frac{2\pi m K_B T}{h^2}\right)^{3/2}$
Internal energy	(24)	$E_{int} = K_B T\left[N_{1s}\frac{\ln\left(\frac{C_e}{Z_v}\right)+n_{1m}\ln\left(\frac{C_1}{C_e}\right)}{1+\left(\frac{C_1}{C_e}\right)^{n_{1m}}}+N_{2s}\frac{\ln\left(\frac{C_e}{Z_v}\right)+n_{2m}\ln\left(\frac{C_2}{C_e}\right)}{1+\left(\frac{C_2}{C_e}\right)^{n_{2m}}}\right]$

The theoretical entropy calculation is displayed in Figure 14a as a function of the MB concentration at various temperatures. As can be shown, entropy behaves very differently according to the MB concentration. Before reaching half-saturation ($C_{1/2} > C$), the entropy increased, indicating a disordered state until it reached a maximum value (Figure 14a). At low MB concentrations, this random state was indicated by the existence of more active sites on the Cs composite that are suited for MB ion adsorption. On the other hand, the entropy increased with increasing MB concentration ($C_{1/2} < C$), indicating an ordered state [63]. The rise in this order state was associated with a decrease in the number of accessible active sites on the Cs material adsorbent [38,64].

Free Gibbs Enthalpy

The free Gibbs enthalpy was determined using Equation (23), stated in Table 7, based on the AM2.

The Gibbs free enthalpy was plotted as a function of the adsorbate concentration at various temperatures for the Cs adsorbent (Figure 14b). As shown in Figure 14b, the Gibbs free energy was negative, showing the spontaneous nature of the adsorption process. Additionally, the feasibility of the adsorption process was reduced as the temperature increased due to the decrease in the free enthalpy [64,65].

Internal Energy

Internal energy can be considered to evaluate all forms of energy provided to the MB adsorption system. Equation (24) in Table 7 gives the general form of the internal

energy [66]. The estimates for this thermodynamic parameter are shown in Figure 14c. The internal energy values were all negative, showing that the MB adsorption systems happened spontaneously [37].

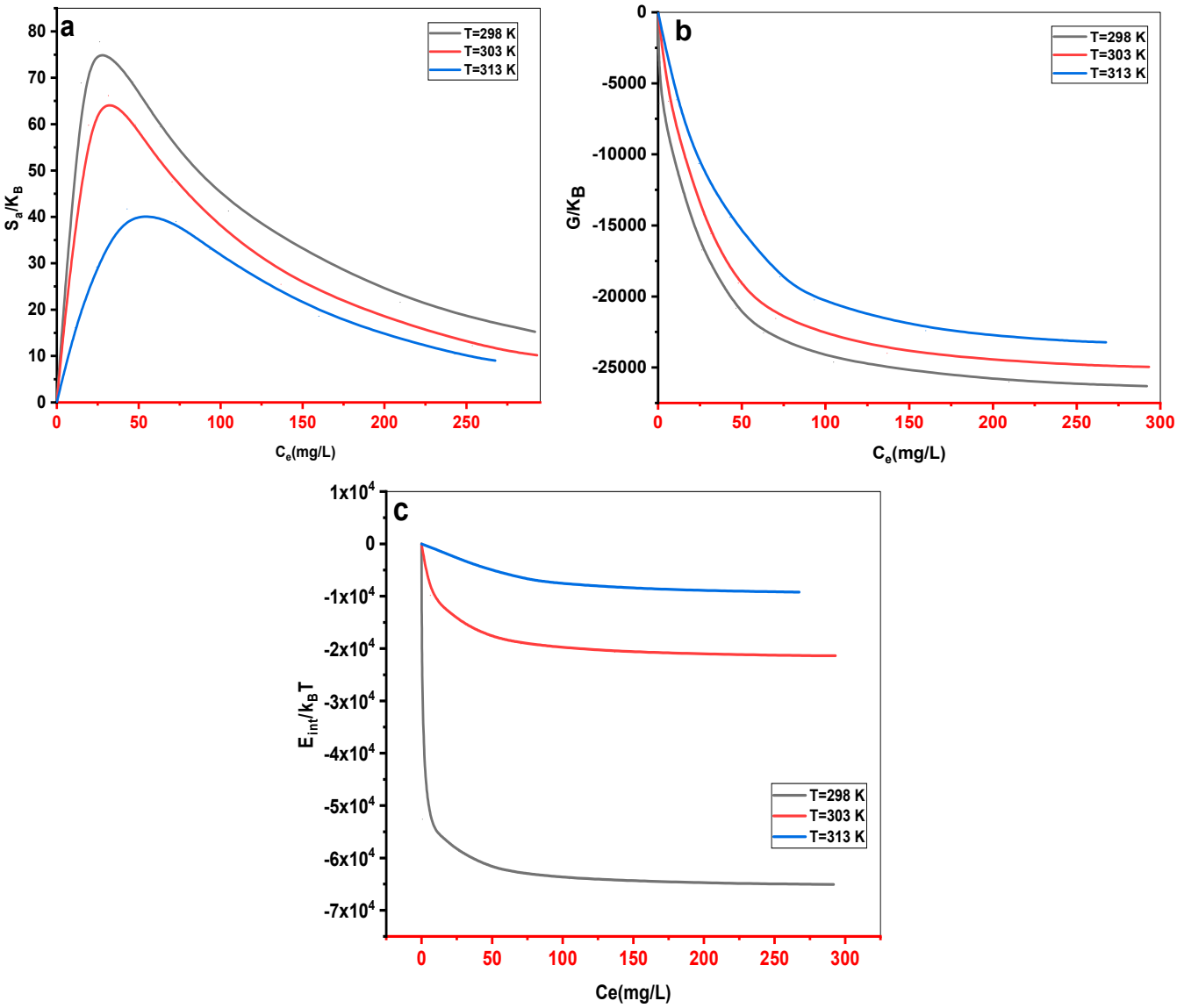

Figure 14. (**a**) Entropy, (**b**) free enthalpy, and (**c**) internal energy evolution as a function of concentration for MB absorption by Cs adsorbent at various temperatures.

3.6. Comparison of Adsorption Capacity with Literature

To prove the effectiveness of *Cynara scolymus* powder as a low-cost biosorbent for MB removal, it is essential to compare its adsorption capacity with that of other low-cost adsorbents. In this study, we compared the adsorption capacity of Cs with other adsorbents reported by various researchers. Numerous studies have been conducted to investigate MB removal from water using different types of adsorbents modified with various chemical agents. The Qmax of these adsorbents is listed in Table 8. The data presented in Table 8 demonstrate that certain materials, such as Acorus calamus (PACK) and Ziziphus jujuba (BZJS), exhibit higher adsorption capacities than *Cynara scolymus* (Cs) powder. It is important to note that PACK is a modified material treated with H2SO4 and subsequently with KMnO4, while BZJS is a material modified with H3PO4 and encapsulated with alginate. These results highlight the relatively low production cost of Cs compared to the aforementioned materials. Furthermore, it is worth noting that the direct powder form of Cs has a

significantly higher maximum adsorption capacity compared to *Cynara scolymus* activated carbon (ACE@CSNB), as indicated in the table. This finding emphasizes the effectiveness and cost-efficiency of Cs as a support material for methylene blue disposal.

Table 8. Comparison of maximum methylene blue adsorption on some literature adsorbents.

Adsorbent Material	Qmax (mg/g)	Reference
PACK	1500	[15]
BZJS1	737.13	[67]
Pectin from orange industry residues in alginate beads form	398.40	[68]
Cynara scolymus Powder (Cs)	203.333	This work
Carboxymethyl cellulose/carboxylated graphene oxide composite microbeads	183.23	[69]
Ziziphus jujuba (PZJS)	160.85	[67]
ACE@CSNB	15	[70]

Overall, the comparison of Cs with other low-cost adsorbents demonstrates its potential as a promising biosorbent for efficient MB removal.

4. Conclusions

The natural powder of *Cynara scolymus* (Cs) was used as an adsorbent in this investigation to remove methylene blue ions (MB). The ideal pH for removing MB color was determined to be 10, which resulted in the greatest amount of adsorption.

The Cs material had a maximum experimental adsorption capacity of 203.333, 192.187, and 179.380 mg•g^{-1} at 298, 303, and 313 K, respectively. Langmuir, Freundlich, Redlich-Peterson (R–P), Sips, and Dubinin–Radushkevich (D–R) were used as classical models to describe experimental results. The Redlich–Peterson (R–P) equation provided the best fit for the adsorption data without elucidating the process of MB absorption. Five statistical physics models (AM1, AM2, AM3, AM4, and AM5) were considered to better explain the interaction between the MB ions and the Cs active sites. The steric, energetic, and thermodynamic parameters resulting from the double-energy single-layer model that gave the appropriate fit of the MB–Cs interaction were thoroughly interpreted. The MB adsorption on the Cs composite was mediated by multi–docking and multimolecular modes. The receptor's site density (N_m) decreased with increasing solution temperature for both N_{m1} and N_{m2}. Adsorption energies were estimated to be negative and <40 kJ•mol^{-1}, indicating exothermic and physical processes. As the temperature dropped, Q_e increased, confirming the exothermic nature of the uptake processes. Entropy, Gibbs free enthalpy, and internal energy indicated that MB adsorption onto the novel Cs adsorbent was possible and spontaneous.

Author Contributions: Conceptualization, C.D., A.B., D.C., A.A., H.T., J.Z. and L.M.; Methodology, C.D., A.B., D.C., A.A., H.T. and L.M.; Software, C.D., A.B., D.C., H.T. and J.Z.; Validation, C.D., A.B., D.C., A.A. and H.T.; Formal analysis, C.D., A.B., D.C., A.A., H.T., J.Z. and L.M.; Investigation, C.D., A.B., D.C., A.A., J.Z. and L.M.; Resources, C.D., A.B., D.C. and L.M.; Data curation, C.D., A.B., D.C., H.T. and J.Z.; Writing—original draft, C.D.; Writing—review & editing, A.B., D.C., A.A., H.T., J.Z. and L.M.; Visualization, C.D., A.B., D.C., A.A., H.T., J.Z. and L.M.; Supervision, A.B., D.C. and A.A.; Project administration, A.B., D.C., A.A. and J.Z. All authors have read and agreed to the published version of the manuscript.

Funding: This research received no external funding.

Acknowledgments: The authors would like to thank the MESRS and DGRSDT (Ministère de l'Enseignement Supérieur et de la Recherche Scientifique et la Direction Générale de la Recherche Scientifique et du Développement Technologique-Algérie) for their financial support.

Conflicts of Interest: The authors declare no conflict of interest.

Nomenclature

Cs	*Cynara scolymus*
C_0	initial concentration of MB (mg•L^{-1})
C_e	final concentration of MB in the solution
C_t	concentration of MB at time t (mg•L^{-1})
C	the intercept of Intraparticle diffusion function
$C_{1/2}$	the concentration at half–saturation (mg•L^{-1})
C_1	concentrations at half saturation for the first active site (mg•L^{-1})
C_2	concentrations at half saturation for the second active site (mg•L^{-1})
E_{DR}	biosorption energy (KJ•mol^{-1})
E_{int}	System internal energy (J•mol^{-1})
F_t	fraction of MB adsorbed at time t
G	Gibbs free enthalpy (J•mol^{-1})
h	Planck constant (J•s^{-1})
K_B	Boltzmann constant (J•K)
k_1	equilibrium rate constant of PFO equation (L•min^{-1})
k_2	equilibrium rate constant of PSO equation (L•min^{-1})
K_{DR}	activity coefficient of Dubinin–Radushkevich isotherm (mol^2•KJ^{-2})
K_F	Freundlich constant (g•L•mg)
k_{id}	the rate constant of intraparticle diffusion(mg•g^{-1}•$min^{-0.5}$)
K_L	Langmuir constant (L•mg^{-1})
k_n	equilibrium rate constant of PNO equation (L•min^{-1})
k_R	Redlich–Peterson (R–P) constant (L•g^{-1})
K_s	Sips constant (L•mg^{-1})
m	mass of the mixture (g)
ms	the exponent of the Sips model
MB	methylene blue
n	number of ions per site
n_1	number of ions per site for the first sites receptor
n_2	number of ions per site for the second sites receptor
nf	Freundlich (R–P) constant
no	biosorption reaction order
N	number of experimental points performed
N_m	sites receptor density(mg•g^{-1})
PFO	pseudo-first-order
PSO	pseudo-second-order
PNO	pseudo-nth-order
Q_e	amount of dye adsorbed at equilibrium (mg•g^{-1})
Q_t	quantity adsorbed at time t (mg•g^{-1})
Q_m	monolayer capacity of the adsorbent (mg•g^{-1})
Qi.mod	model's adsorbate adsorption capacity (mg•g^{-1})
Qi.exp	experimental adsorption capacity (mg•g^{-1})
S_a	Entropy (J•mol•K^{-1})
t	time (min)
T	temperature (K)
V	volume of the mixture (L)
Z_v	Translation partition function per unit volume
Z_{gtr}	translation partition function
α_R	constant of the Redlich–Peterson isotherm (L•mg•g^{-1})
β_R	constant of the Redlich–Peterson isotherm
β_t	mathematical function of F_t
ε	constant related to the adsorption energy for Dubinin–Radushkevich isotherm

References

1. Bouguettoucha, A.; Chebli, D.; Mekhalef, T.; Noui, A.; Amrane, A. The use of a forest waste biomass, cone of *Pinus brutia* for the removal of an anionic azo dye Congo red from aqueous medium. *Desalin. Water Treat.* **2015**, *55*, 1956–1965. [CrossRef]
2. Bouguettoucha, A.; Reffas, A.; Chebli, D.; Mekhalif, T.; Amrane, A. Novel activated carbon prepared from an agricultural waste, *Stipa tenacissima*, based on $ZnCl_2$ activation—Characterization and application to the removal of methylene blue. *Desalin. Water Treat.* **2016**, *57*, 24056–24069. [CrossRef]
3. Tsai, W.T.; Chang, Y.M.; Lai, C.W.; Lo, C.C. Adsorption of ethyl violet dye in aqueous solution by regenerated spent bleaching earth. *J. Colloid Interface Sci.* **2005**, *289*, 333–338. [CrossRef]
4. Bhattacharyya, K.G.; Sharma, A. Kinetics and thermodynamics of methylene blue adsorption on neem (*Azadirachta indica*) leaf powder. *Dye Pigment.* **2005**, *65*, 51–59. [CrossRef]
5. Srinivasan, A.; Viraraghavan, T. Decolorization of dye wastewaters by biosorbents: A review. *J. Environ. Manag.* **2010**, *91*, 1915–1929. [CrossRef]
6. Yao, Z.; Wang, L.; Qi, J. Biosorption of methylene blue from aqueous solution using a bioenergy forest waste: *Xanthoceras sorbifolia* seed coat. *CLEAN Soil Air Water* **2009**, *37*, 642–648. [CrossRef]
7. Guediri, A.; Bouguettoucha, A.; Chebli, D.; Chafai, N.; Amrane, A. Molecular dynamic simulation and DFT computational studies on the adsorption performances of methylene blue in aqueous solutions by orange peel-modified phosphoric acid. *J. Mol. Struct.* **2020**, *1202*, 127290. [CrossRef]
8. Crini, G. Non-conventional low-cost adsorbents for dye removal: A review. *Bioresour. Technol.* **2006**, *97*, 1061–1085. [CrossRef] [PubMed]
9. Chebli, D.; Bouguettoucha, A.; Mekhalef, T.; Nacef, S.; Amrane, A. Valorization of an agricultural waste, *Stipa tenassicima* fibers, by biosorption of an anionic azo dye, Congo red. *Desalin. Water Treat.* **2015**, *54*, 245–254. [CrossRef]
10. Cardoso, N.F.; Lima, E.C.; Pinto, I.S.; Amavisca, C.V.; Royer, B.; Pinto, R.B.; Alencar, W.S.; Pereira, S.F.P. Application of cupuassu shell as biosorbent for the removal of textile dyes from aqueous solution. *J. Environ. Manag.* **2011**, *92*, 1237–1247. [CrossRef]
11. Naiya, T.K.; Chowdhury, P.; Bhattacharya, A.K.; Das, S.K. Saw dust and neem bark as low-cost natural biosorbent for adsorptive removal of Zn (II) and Cd (II) ions from aqueous solutions. *Chem. Eng. J.* **2009**, *148*, 68–79. [CrossRef]
12. Ben-Ali, S.; Jaouali, I.; Souissi-Najar, S.; Ouederni, A. Characterization and adsorption capacity of raw pomegranate peel biosorbent for copper removal. *J. Clean. Prod.* **2017**, *142*, 3809–3821. [CrossRef]
13. Southichak, B.; Nakano, K.; Nomura, M.; Chiba, N.; Nishimura, O. Phragmites australis: A novel biosorbent for the removal of heavy metals from aqueous solution. *Water Res.* **2006**, *40*, 2295–2302. [CrossRef] [PubMed]
14. Aravindhan, R.; Rao, J.R.; Nair, B.U. Application of a chemically modified green macro alga as a biosorbent for phenol removal. *J. Environ. Manag.* **2009**, *90*, 1877–1883. [CrossRef] [PubMed]
15. Djama, C.; Chebli, D.; Bouguettoucha, A.; Doudou, I.; Amrane, A. Statistical physics modelling of azo dyes biosorption onto modified powder of *Acorus calamus* in batch reactor. *Biomass Convers. Biorefinery* **2021**, *13*, 1–16. [CrossRef]
16. Pandino, G.; Lombardo, S.; Monaco, A.L.; Mauromicale, G. Choice of time of harvest influences the polyphenol profile of globe artichoke. *J. Funct. Foods* **2013**, *5*, 1822–1828. [CrossRef]
17. Salem, M.B.; Affes, H.; Ksouda, K.; Dhouibi, R.; Sahnoun, Z.; Hammami, S.; Zeghal, K.M. Pharmacological studies of artichoke leaf extract and their health benefits. *Plant Foods Hum. Nutr.* **2015**, *70*, 441–453. [CrossRef]
18. Saavedra, M.I.; Miñarro, M.D.; Angosto, J.M.; Fernandez-Lopez, J.A. Reuse potential of residues of artichoke (*Cynara scolymus* L.) from industrial canning processing as sorbent of heavy metals in multimetallic effluents. *Ind. Crops Prod.* **2019**, *141*, 111751. [CrossRef]
19. Mahmoud, M.E.; Abou-Ali, S.A.A.; Elweshahy, S.M.T. Efficient and ultrafast removal of Cd (II) and Sm (III) from water by leaves of *Cynara scolymus* derived biochar. *Mater. Res. Bull.* **2021**, *141*, 111334. [CrossRef]
20. Mobarak, M.; Mohamed, E.; Selim, A.; Sellaoui, L.; Lamine, A.B.; Erto, A.; Seliem, M.K. Surfactant–modified serpentine for fluoride and Cr (VI) adsorption in single and binary systems: Experimental studies and theoretical modeling. *Chem. Eng. J.* **2019**, *369*, 333–343. [CrossRef]
21. Mobarak, M.; Mohamed, E.A.; Selim, A.Q.; Mohamed, F.M.; Sellaoui, L.; Bonilla-Petriciolet, A.; Seliem, M.K. Statistical physics modeling and interpretation of methyl orange adsorption on high–order mesoporous composite of MCM–48 silica with treated rice husk. *J. Mol. Liq.* **2019**, *285*, 678–687. [CrossRef]
22. Sellaoui, L.; Bouzid, M.; Duclaux, L.; Reinert, L.; Knani, S.; Lamine, A.B. Binary adsorption isotherms of two ionic liquids and ibuprofen on an activated carbon cloth: Simulation and interpretations using statistical and COSMO-RS models. *RSC Adv.* **2016**, *6*, 67701–67714. [CrossRef]
23. Li, Z.; Sellaoui, L.; Dotto, G.L.; Lamine, A.B.; Bonilla-Petriciolet, A.; Hanafy, H.; Belmabrouk, H.; Netto, M.S.; Erto, A. Interpretation of the adsorption mechanism of Reactive Black 5 and Ponceau 4R dyes on chitosan/polyamide nanofibers via advanced statistical physics model. *J. Mol. Liq.* **2019**, *285*, 165–170. [CrossRef]
24. Sellaoui, L.; Soetaredjo, F.E.; Ismadji, S.; Lima, É.C.; Dotto, G.L.; Lamine, A.B.; Erto, A. New insights into single-compound and binary adsorption of copper and lead ions on a treated sea mango shell: Experimental and theoretical studies. *Phys. Chem. Chem. Phys.* **2017**, *19*, 25927–25937. [CrossRef]
25. Lamine, A.B.; Bouazra, Y. Application of statistical thermodynamics to the olfaction mechanism. *Chem. Senses* **1997**, *22*, 67–75. [CrossRef] [PubMed]

26. Yahia, M.B.; Tounsi, M.; Aouaini, F.; Knani, S.; Yahia, M.B.; Lamine, A.B. A statistical physics study of the interaction of [7]-helicene with alkali cations (K+ and Cs+): New insights on microscopic adsorption behavior. *RSC Adv.* **2017**, *7*, 44712–44723. [CrossRef]
27. Xue, H.; Gao, X.; Seliem, M.K.; Mobarak, M.; Dong, R.; Wang, X.; Fu, K.; Li, Q.; Li, Z. Efficient adsorption of anionic azo dyes on porous heterostructured MXene/biomass activated carbon composites: Experiments, characterization, and theoretical analysis via advanced statistical physics models. *Chem. Eng. J.* **2023**, *451*, 138735. [CrossRef]
28. Sellaoui, L.; Gomez-Aviles, A.; Dhaouadi, F.; Bedia, J.; Bonilla-Petriciolet, A.; Rtimi, S.; Belver, C. Adsorption of emerging pollutants on lignin-based activated carbon: Analysis of adsorption mechanism via characterization, kinetics and equilibrium studies. *Chem. Eng. J.* **2023**, *452*, 139399. [CrossRef]
29. Wang, X.; Xu, Q.; Zhang, L.; Pei, L.; Xue, H.; Li, Z. Adsorption of methylene blue and Congo red from aqueous solution on 3D MXene/carbon foam hybrid aerogels: A study by experimental and statistical physics modeling. *J. Environ. Chem. Eng.* **2023**, *11*, 109206. [CrossRef]
30. Gómez-Avilés, A.; Sellaoui, L.; Badawi, M.; Bonilla-Petriciolet, A.; Bedia, J.; Belver, C. Simultaneous adsorption of acetaminophen, diclofenac and tetracycline by organo-sepiolite: Experiments and statistical physics modelling. *Chem. Eng. J.* **2021**, *404*, 126601. [CrossRef]
31. Shamsudin, M.S.; Azha, S.F.; Sellaoui, L.; Badawi, M.; Bonilla-Petriciolet, A.; Ismail, S. Performance and interactions of diclofenac adsorption using Alginate/Carbon-based Films: Experimental investigation and statistical physics modelling. *Chem. Eng. J.* **2022**, *428*, 131929. [CrossRef]
32. Al-Yousef, H.A.; Alotaibi, B.M.; Aouaini, F.; Sellaoui, L.; Bonilla-Petriciolet, A. Adsorption of ibuprofen on cocoa shell biomass-based adsorbents: Interpretation of the adsorption equilibrium via statistical physics theory. *J. Mol. Liq.* **2021**, *331*, 115697. [CrossRef]
33. Sellaoui, L.; Dhaouadi, F.; Reynel-Avila, H.E.; Mendoza-Castillo, D.I.; Bonilla-Petriciolet, A.; Trejo-Valencia, R.; Taamalli, S.; Louis, F.; El Bakali, A.; Chen, Z. Physicochemical assessment of anionic dye adsorption on bone char using a multilayer statistical physics model. *Environ. Sci. Pollut. Res.* **2021**, *28*, 67248–67255. [CrossRef] [PubMed]
34. Sarra, A.; Chaker, D.; Abdallah, B.; Derradji, C.; Abdeltif, A. Adsorption of a Cationic Dye Crystal Violet onto a Binary Mixture of Forest Waste Biopolymer: Advanced Statistical Physics Studies. *Adv. Mater. Res.* **2022**, *1168*, 93–113. [CrossRef]
35. Tseng, R.-L.; Wu, P.-H.; Wu, F.-C.; Juang, R.-S. A convenient method to determine kinetic parameters of adsorption processes by nonlinear regression of pseudo-nth-order equation. *Chem. Eng. J.* **2014**, *237*, 153–161. [CrossRef]
36. Oladipo, A.A.; Gazi, M. Enhanced removal of crystal violet by low cost alginate/acid activated bentonite composite beads: Optimization and modelling using non-linear regression technique. *J. Water Process Eng.* **2014**, *2*, 43–52. [CrossRef]
37. Sadeghi, G.M.M.; Shamsi, R.; Sayaf, M. From Aminolysis Product of PET Waste to Novel Biodegradable Polyurethanes. *J. Polym. Environ.* **2011**, *19*, 522–534. [CrossRef]
38. Feng, J.; Liu, R.; Chen, P.; Yuan, S.; Zhao, D.; Zhang, J.; Zheng, Z. Degradation of aqueous 3,4-dichloroaniline by a novel dielectric barrier discharge plasma reactor. *Environ. Sci. Pollut. Res.* **2015**, *22*, 4447–4459. [CrossRef]
39. Ahmadpoor, F.; Shojaosadati, S.A.; Mousavi, S.Z. Magnetic silica coated iron carbide/alginate beads: Synthesis and application for adsorption of Cu (II) from aqueous solutions. *Int. J. Biol. Macromol.* **2019**, *128*, 941–947. [CrossRef]
40. Yazidi, A.; Sellaoui, L.; Dotto, G.L.; Bonilla-Petriciolet, A.; Fröhlich, A.C.; Lamine, A.B. Monolayer and multilayer adsorption of pharmaceuticals on activated carbon: Application of advanced statistical physics models. *J. Mol. Liq.* **2019**, *283*, 276–286. [CrossRef]
41. Guechi, E.-K.; Hamdaoui, O. Sorption of malachite green from aqueous solution by potato peel: Kinetics and equilibrium modeling using non-linear analysis method. *Arab. J. Chem.* **2016**, *9*, S416–S424. [CrossRef]
42. Rangabhashiyam, S.; Selvaraju, N. Adsorptive remediation of hexavalent chromium from synthetic wastewater by a natural and ZnCl2 activated *Sterculia guttata* shell. *J. Mol. Liq.* **2015**, *207*, 39–49. [CrossRef]
43. Khodabandehloo, A.; Rahbar-Kelishami, A.; Shayesteh, H. Methylene blue removal using *Salix babylonica* (Weeping willow) leaves powder as a low-cost biosorbent in batch mode: Kinetic, equilibrium, and thermodynamic studies. *J. Mol. Liq.* **2017**, *244*, 540–548. [CrossRef]
44. Akar, T.; Anilan, B.; Gorgulu, A.; Akar, S.T. Assessment of cationic dye biosorption characteristics of untreated and non-conventional biomass: *Pyracantha coccinea* berries. *J. Hazard. Mater.* **2009**, *168*, 1302–1309. [CrossRef] [PubMed]
45. Rangabhashiyam, S.; Lata, S.; Balasubramanian, P. Biosorption characteristics of methylene blue and malachite green from simulated wastewater onto *Carica papaya* wood biosorbent. *Surf. Interfaces* **2018**, *10*, 197–215.
46. Lopičić, Z.R.; Stojanović, M.D.; Marković, S.B.; Milojković, J.V.; Mihajlović, M.L.; Radoičić, T.S.K.; Kijevčanin, M.L. Effects of different mechanical treatments on structural changes of lignocellulosic waste biomass and subsequent Cu (II) removal kinetics. *Arab. J. Chem.* **2019**, *12*, 4091–4103. [CrossRef]
47. El Amri, A.; Bensalah, J.; Idrissi, A.; Lamya, K.; Ouass, A.; Bouzakraoui, S.; Zarrouk, A.; Lebkiri, A. Adsorption of a cationic dye (Methylene bleu) by *Typha Latifolia*: Equilibrium, kinetic, thermodynamic and DFT calculations. *Chem. Data Collect.* **2022**, *38*, 100834. [CrossRef]
48. Postai, D.L.; Rodrigues, C.A. Adsorption of cationic dyes using waste from fruits of *Eugenia umbelliflora Berg* (*Myrtaceae*). *Arab. J. Sci. Eng.* **2018**, *43*, 2425–2440. [CrossRef]
49. Namasivayam, C.; Kavitha, D. XRD and SEM studies on the mechanism of adsorption of dyes and phenols by coir pith carbon from aqueous phase. *Microchem. J.* **2006**, *82*, 43–48. [CrossRef]

50. Luo, W.-J.; Gao, Q.; Wu, X.-L.; Zhou, C.-G. Removal of cationic dye (methylene blue) from aqueous solution by humic acid-modified expanded perlite: Experiment and theory. *Sep. Sci. Technol.* **2014**, *49*, 2400–2411. [CrossRef]
51. Amri, A.E.L.; Bensalah, J.; Essaadaoui, Y.; Lebkiri, I.; Abbou, B.; Zarrouk, A.; Lebkiri, A. Elaboration, characterization and performance evaluation of a new environmentally friendly adsorbent material based on the reed filter (*Typha Latifolia*): Kinetic and thermodynamic studies and application in the adsorption of Cd (II) ion. *Chem. Data Collect.* **2022**, *39*, 100849. [CrossRef]
52. Bensalah, J.; Berradi, M.; Habsaoui, A.; Allaoui, M.; Essebaai, H.; El Khattabi, O.; Lebkiri, A.; Rifi, E.-H. Kinetic and thermodynamic study of the adsorption of cationic dyes by the cationic artificial resin Amberlite® IRC50. *Mater. Today Proc.* **2021**, *45*, 7468–7472. [CrossRef]
53. Bensalah, J.; Benhiba, F.; Habsaoui, A.; Ouass, A.; Zarrouk, A.; Lebkiri, A.; El Khattabi, O. The adsorption mechanism of the anionic and cationic dyes of the cationic resin A® IRC-50, kinetic study and theoretical investigation using DFT. *J. Indian Chem. Soc.* **2022**, *99*, 100512. [CrossRef]
54. Bensalah, J.; Idrissi, A.; El Faydy, M.; Doumane, G.; Staoui, A.; Hsissou, R.; Lebkiri, A.; Habsaoui, A.; Abdelkader, Z. Investigation of the cationic resin as a potential adsorbent to remove MR and CV dyes: Kinetic, equilibrium isotherms studies and DFT calculations. *J. Mol. Struct.* **2023**, 134849. [CrossRef]
55. Li, S.; Zeng, Z.; Xue, W. Adsorption of lead ion from aqueous solution by modified walnut shell: Kinetics and thermodynamics. *Environ. Technol.* **2019**, *40*, 1810–1820. [CrossRef]
56. Kumar, A.S.K.; Warchol, J.; Matusik, J.; Tseng, W.-L.; Rajesh, N.; Bajda, T. Heavy metal and organic dye removal via a hybrid porous hexagonal boron nitride-based magnetic aerogel. *NPJ Clean Water* **2022**, *5*, 24. [CrossRef]
57. Elabboudi, M.; Bensalah, J.; El Amri, A.; Azzouzi, N.E.L.; Srhir, B.; Zarrouk, A. Adsorption performance and mechanism of anionic MO dye by the adsorbent polymeric Amberlite® IRA-410 resin from environment wastewater: Equilibrium kinetic and thermodynamic studies. *J. Mol. Struct.* **2023**, *1277*, 134789. [CrossRef]
58. Silva, L.S.; Lima, L.C.B.; Ferreira, F.J.L.; Silva, M.S.; Osajima, J.A.; Bezerra, R.D.S.; Filho, E.C.S. Sorption of the anionic reactive red RB dye in cellulose: Assessment of kinetic, thermodynamic, and equilibrium data. *Open Chem.* **2015**, *13*, 801–812. [CrossRef]
59. Kumar, K.V.; Sivanesan, S. Equilibrium data, isotherm parameters and process design for partial and complete isotherm of methylene blue onto activated carbon. *J. Hazard. Mater.* **2006**, *134*, 237–244. [CrossRef]
60. Selim, A.Q.; Sellaoui, L.; Mobarak, M. Statistical physics modeling of phosphate adsorption onto chemically modified carbonaceous clay. *J. Mol. Liq.* **2019**, *279*, 94–107. [CrossRef]
61. Sellaoui, L.; Dotto, G.L.; Peres, E.C.; Benguerba, Y.; Lima, É.C.; Lamine, A.B.; Erto, A. New insights into the adsorption of crystal violet dye on functionalized multi-walled carbon nanotubes: Experiments, statistical physics and COSMO–RS models application. *J. Mol. Liq.* **2017**, *248*, 890–897. [CrossRef]
62. Stovall, M.; Smith, S.A.; Langholz, B.M.; Boice, J.D., Jr.; Shore, R.E.; Andersson, M.; Buchholz, T.A.; Capanu, M.; Bernstein, L.; Lynch, C.F. Dose to the contralateral breast from radiotherapy and risk of second primary breast cancer in the WECARE study. *Int. J. Radiat. Oncol. Biol. Phys.* **2008**, *72*, 1021–1030. [CrossRef]
63. Sellaoui, L.; Guedidi, H.; Knani, S.; Reinert, L.; Duclaux, L.; Lamine, A.B. Application of statistical physics formalism to the modeling of adsorption isotherms of ibuprofen on activated carbon. *Fluid Phase Equilib.* **2015**, *387*, 103–110. [CrossRef]
64. Khalfaoui, M.; Knani, S.; Hachicha, M.A.; Lamine, A.B. New theoretical expressions for the five adsorption type isotherms classified by BET based on statistical physics treatment. *J. Colloid Interface Sci.* **2003**, *263*, 350–356. [CrossRef] [PubMed]
65. Mobarak, M.; Mohamed, E.A.; Selim, A.Q.; Eissa, M.F.; Seliem, M.K. Experimental results and theoretical statistical modeling of malachite green adsorption onto MCM–41 silica/rice husk composite modified by beta radiation. *J. Mol. Liq.* **2019**, *273*, 68–82. [CrossRef]
66. Sellaoui, L.; Li, Z.; Badawi, M.; Dotto, G.L.; Bonilla-Petriciolet, A.; Chen, Z. Origin of the outstanding performance of ZnAl and MgFe layered double hydroxides in the adsorption of 2-nitrophenol: A statistical physics assessment. *J. Mol. Liq.* **2020**, *314*, 113572. [CrossRef]
67. Guediri, A.; Bouguettoucha, A.; Chebli, D.; Amrane, A. The use of encapsulation as a proposed solution to avoid problems encountered with conventional materials in powder form: Application in methylene blue removal from aqueous solutions. *J. Mol. Liq.* **2020**, *316*, 113841. [CrossRef]
68. Kebaili, M.; Djellali, S.; Radjai, M.; Drouiche, N.; Lounici, H. Valorization of orange industry residues to form a natural coagulant and adsorbent. *J. Ind. Eng. Chem.* **2018**, *64*, 292–299. [CrossRef]
69. Eltaweil, A.S.; Elgarhy, G.S.; El-Subruiti, G.M.; Omer, A.M. Carboxymethyl cellulose/carboxylated graphene oxide composite microbeads for efficient adsorption of cationic methylene blue dye. *Int. J. Biol. Macromol.* **2020**, *154*, 307–318. [CrossRef]
70. Mahmoud, S.E.M.E.; Ursueguia, D.; Mahmoud, M.E.; Abel-Fattah, T.M.; Díaz, E. Functional surface homogenization of nanobiochar with cation exchanger for improved removal performance of methylene blue and lead pollutants. *Biomass Convers. Biorefinery* **2023**, 1–21. [CrossRef]

Disclaimer/Publisher's Note: The statements, opinions and data contained in all publications are solely those of the individual author(s) and contributor(s) and not of MDPI and/or the editor(s). MDPI and/or the editor(s) disclaim responsibility for any injury to people or property resulting from any ideas, methods, instructions or products referred to in the content.